N71-15082

NASA CR-72794

AVSD-0629-70-RR

HIGH TEMPERATURE COMPOUNDS FOR TURBINE VANES

by

R.M. Cannon, Jr. and R.J. Hill

AVCO CORPORATION
Lowell, Massachusetts

prepared for

NATIONAL AERONAUTICS AND SPACE ADMINISTRATION

NASA Lewis Research Center

Contract NAS3-13213
William A. Sanders, Project Manager

## NOTICE

This report was prepared as an account of Government-sponsored work. Neither the United States, nor the National Aeronautics and Space Administration (NASA), nor any person acting on behalf of NASA:

A.) Makes any warranty or representation, expressed, implied, with respect to the accuracy, completeness or usefulness of the information contained in this report, or that the use of any information, apparatus, method, or process disclosed in this report may not infringe privately-owned rights; or

B.) Assumes any liabilities with respect to the use of, or for damages resulting from the use of, any information, apparatus, method or process disclosed in this report.

As used above, "person acting on behalf of NASA" includes any employee or contractor of NASA, or employee of such contractor, to the extent that such employee or contractor of NASA or employee of such contractor prepares, disseminates, or provides access to any information pursuant to his employment or contract with NASA, or his employment with such contractor.

Requests for copies of this report should be referred to

National Aeronautics and Space Administration
Scientific and Technical Information Facility
P.O. Box 33
College Park, Md. 20740

FINAL REPORT

HIGH TEMPERATURE COMPOUNDS FOR TURBINE VANES

by

R.M. Cannon, Jr. and R.J. Hill

AVCO CORPORATION
Lowell Industrial Park
Lowell, Massachusetts 01851

prepared for

NATIONAL AERONAUTICS AND SPACE ADMINISTRATION

August 31, 1970

## FOREWORD

The research described herein, which was conducted by the Avco Corporation, Systems Division, was performed under NASA Contract NAS3-13213. The work was done under the management of the NASA Project Manager, Mr. William A. Sanders, Materials & Structures Division, NASA Lewis Research Center with Dr. Russell J. Hill, Materials Sciences Department, Avco Corporation as Principal Investigator.

# ABSTRACT

A number of fibrous additives were incorporated into both silicon carbide and silicon nitride ceramic matrices and consolidated by hot pressing methods. The properties of the composites were investigated to determine if any improvement of mechanical properties had resulted. Impact strength was measured in air up to 2400°F in the Charpy mode and stress rupture lives were also measured in air in four-point bending for temperatures up to 2400°F. These data were compared with data obtained under identical conditions for some superalloys. The thermal shock and thermochemical stability characteristics were also determined under simulated gas turbine stator vane environments at 2400°F.

It was concluded that the incorporation of SiC whiskers into both SiC and $Si_3N_4$ matrices markedly increases the impact strength in the range of room temperature to 2400°F without seriously detracting from the mechanical, thermal shock or thermochemical stability characteristics of the ceramic matrix.

# TABLE OF CONTENTS

FOREWORD

ABSTRACT

# LIST OF ILLUSTRATIONS

# LIST OF ILLUSTRATIONS (Concl'd)

Figure No.

# LIST OF TABLES

# I. SUMMARY

The objective of this program was to determine the feasibility of improving the mechanical behavior of high temperature composites to such a degree that they become materials for use as turbine stator vanes in advanced turbine engines. The high temperature compound systems studied where SiC and $Si_3N_4$ alone and with additions of fibrous materials such as SiC whiskers to make composites. The program sought to improve the mechanical impact resistance (which was of primary importance), the thermal shock resistance and the stress-rupture life of these high temperature composites.

The high temperature composite process development aim was to produce composites, which would demonstrate stability so that no serious decomposition vaporization, change of composition, loss of stabilizer, etc., would occur under cyclic exposure to air from room temperature to elevated temperature.

The composites were made using the hot pressing method. Additive loading was from 10 up to 50 volume percent. The parameters of pressure, temperature, time were selected and modified in accordance with densification behavior of the systems and the mechanical property behavior of the composites resulting therefrom.

The composites were tested to measure their thermal shock resistance and stability in air for long times under cyclic temperature conditions. The mechanical shock resistance was also measured in air at a number of high temperatures. Finally, the stress-rupture lives of those composites which showed promise in the preceding tests were measured at high temperatures in a bending mode.

SiC and $Si_3N_4$ made by hot pressing and having certain sintering aid additions are capable of successfully surviving at least 100 cycles in a simulated gas turbine stator vane environment at $2400^\circ$F ($1589^\circ$K). Additions of SiC whiskers do not have a marked effect on the thermal stability/shock resistance of either SiC or $Si_3N_4$. In terms of impact strength there is a marked increase when SiC whiskers are added to either ceramic to form a composite. The impact strength of SiC does not change much at high temperature compared with the room temperature values. Silicon nitride has a higher impact strength than SiC. The strength of $Si_3N_4$ also increased when heated to $2000^\circ$F ($1366^\circ$K) and $2400^\circ$F ($1589^\circ$K).

At $2000^\circ$F ($1366^\circ$K) the $Si_3N_4$ had the highest rupture strength of all the materials tested. At $2400^\circ$F ($1589^\circ$K) the SiC based materials were superior. Indications are that reducing the residual grain boundary impurities would extend the temperature capability of $Si_3N_4$; this would be expected to result in substantial improvements in the $2400^\circ$F ($1589^\circ$K) stress rupture strength. Although beneficial in terms of impact strength, some loss in stress rupture properties result from the addition of whiskers.

The work reported indicated that in terms of most of the critical requirements, ceramic composites based on SiC or·$Si_3N_4$ show promise for use in low stress areas of gas turbines at least up to $2400^\circ$F ($1589^\circ$K). Despite being inherently brittle materials, their fracture toughness has been improved

by additions of SiC whiskers. When these additions can be optimized, it is anticipated that the composites can compete successfully with metals for stator vanes in advanced gas turbines.

## II. INTRODUCTION

The conditions turbine blades and vanes can withstand determine to a large extent the ultimate performance of a gas turbine. Although the burner may run at somewhat higher temperature than the blades and vanes, the mechanical stresses involved are less and so any increase in capabilities of mechanical, chemical and thermal properties of the active members represents an increase in turbine performance. It is projected that the turbine inlet temperatures in the 1970's will exceed the melting points of the currently used nickel or cobalt-based alloys. For the dynamic blade structures involving high centrifugal forces, transpirational cooling may be the solution. However, for vanes, where lower stresses are involved, the use of inherently stable, refractory, oxidation-resistant materials would provide a reasonable solution. There have been indications that at least two materials, silicon carbide and silicon nitride, have almost all of the necessary properties for this function including oxidation resistance, thermal shock resistance, strength, stress rupture life and chemical stability. However, the impact strength of ceramic materials is notoriously low and the values for $SiC$ and $Si_3N_4$ are no exception. A number of methods can, however, be used to improve the fracture toughness of ceramics and at least one of these, the use of fibrous composite techniques, does not detract from the other properties necessary for use as gas turbine vanes.

The continued development of modern fiber composite materials originates with the development of glass fiber reinforced plastics during the early 1940's. At first, the only method available for the fabrication of composite components consisted of soaking glass fiber cloth or mat with thermosetting polymers. More sophisticated fabricating techniques have been developed since then, one of which is the winding of continuous filaments. The utilization of glass fiber reinforced plastics is now commonplace and a commercial success.

Metallic filaments have been used to increase impact strengths of ceramic materials. Wire mesh in glass is a familiar example. For high temperature ablators a metallic honeycomb material has been filled with silica and hot pressed to provide ahigh thermal stress resistant material (Avcoite I) and has been used for a number of years at Avco. The requirements of such materials are such that the two components be compatible at the hot pressing temperature and also the metal will not lose its mechanical properties by loss of ductility due to grain growth or similar mechanisms as a result of the high temperature treatment.

The discovery of "whiskers" or short fibers that are very strong[1] and that the strength properties of fiber reinforced composites containing either continuous or discontinuous fibers was basically the same,[2,3] (law of mixtures for strength) has pointed the way towards the development of high strength, low density, high modulus filaments. The basic modulus of a composite was shown to depend upon the relative volume fraction and moduli of the components.

A number of different high modulus filaments have been developed and are currently being brought into production. In addition, methods by which these filaments may be utilized are being developed. These methods include incorporation of the filaments in metal as well as plastic matrices. Limited

data indicate that fibrous components with ceramic matrices have improved impact strength and thermal shock properties over the original ceramic. It is not proposed to review these data here since a recent review of the field[4] by Bowen describes much of the work done up until 1968. Suffice it to say that improvements in impact strength of ceramic matrices have been reported when ceramic fibrous additions have been made.

The approach used was to determine the effect of high strength filamentary additives on the properties of ceramic materials already having many high-grade qualities. The two ceramic materials chosen were silicon carbide and silicon nitride. The composites were fabricated by conventional hot pressing techniques adjusted where necessary to allow proper micro-structural control to be effected. A number of additives were used and their success was judged by subjecting the resultant composite to tests and simulated environments which resembled as far as possible in the laboratory those conditions prevailing in an advanced gas turbine. Although ultimately high impact strength and high creep strength were the goals, all candidate composites were required to pass a test involving high temperature thermo-chemical stability and thermal shock.

III.  COMPOSITE FABRICATION

     All composites were fabricated by hot pressing using graphite die bodies and pistons.  It was very important to know the temperature of hot pressing particularly when filamentary additions having high surface energies were added to a matrix and when a temperature close to an interaction temperature between the components was often necessary for consolidation.  A typical hot pressing set up of the size used for 2" diameter billets and of the overall size of die body also used for 3" diameter billets, was used to calibrate the temperature normally measured during a hot pressing and the temperature after hot pressing.

     The results of a temperature calibration experiment are summarized in Appendix A.

     Some cooperative non-destructive testing (NDT) of billets fabricated in this program was performed under another program.[5]  Radiometric densities for 15 positions on the billet were measured, together with a qualitative estimate of surface cracks using dye penetrant techniques.  The dynamic elastic modulus was also found using sonic velocity determinations for certain selected billets.  The NDT results for the billets examined are shown in Table 2 for SiC and Table 5 for $Si_3N_4$.  The density variability was taken as a percentage over the 15 radiometric gagings.  Ultrasonically measured moduli are also reported.

    A.  Silicon Carbide Fabrication

       1.  Powder Characterization

     To obtain a high density, fine-grained silicon carbide body, previous work[6] has shown that certain additives are necessary.  It was supposed that these additives remove impurities present in the starting powder such as silicon and silica which ordinarily promote grain growth.  The SiC used was the Carborundum SIKA grade obtained in the 1000 grit size.  The analysis of the powder by x-ray diffraction (Debye-Scherrer) showed the major phases to consist of $\alpha$-SiC (form II) with a minor amount of $\alpha$-SiC (form I).  The $\beta$-SiC may be present as a minor phase, although this cannot be definitely established due to coincidence of the strongest cubic lines ( $\beta$-SiC) with those of the hexagonal form ( $\alpha$-SiC).  The hot pressed material has been analyzed in the case of billet 1275 using the x-ray diffractometer technique on a surface cut parallel with the pressing direction. The sample was best identified as  $\alpha$-SiC (form III) with a minor amount of $\alpha$-SiC (form II) with some $\alpha$-SiC (form VI) with no $\beta$-SiC detected. Thus, the $\alpha$-form is retained during hot pressing, confirming the work of Alliegro[6], although the type of stacking polymorph changes from principally form II to the form III.

     The impurities present were at concentrations below those limits applicable to x-ray diffraction.  Carborundum Company provided information regarding the particular batch of powder used in this program as being:

        Silicon  0.02%
        $SiO_2$    0.86%

An electron micrograph of the powder mode and an average particle size determined to be 6.2 $\mu$m. A portion of the micrograph is shown in Figure 1.

### 2. Hot Pressing

After mixing the SiC powder and additives, each mixture was hot pressed in a graphite die material under the conditions described in Table 1 for each billet.

### a. Densification Additives

A number of variations in additions were made initially to determine the optimum conditions for the particular powder batch used so that a dense, fine-grained material could be obtained. Both $Al_2O_3$ and $Fe_2O_3$ were used separately and together (see billets 1209, 1211, 1221A, 1225), but it was found that a high density could not be obtained. Further, a material having no additive could be pressed to a higher density (see billet 1223A) under similar conditions. It should be noted that the pressings are made 'to zero movement' of the punches, (which may, however, at temperatures above 3812°F (2373°K) amount to some finite strain-rate which is due to creep in the graphite piston train). Different pressing times should, therefore, not necessarily be construed, per se, as being a different pressing condition, since small temperature variations can account for large differences in pressing times.

A typical microstructure of a SiC billet with 3 w/o $Al_2O_3$ additive is shown in Figure 2. Although the section is heavily stained, the large grained structure is strongly in evidence with large porosity contributing to the low density of billet 1224. The SiC is electrolytically etched in KOH solution. When $Fe_2O_3$ and $Al_2O_3$ additions are both made to SiC, both as 3 w/o in billet 1225A, a finer-grained structure results as shown in Figure 3. A lightly colored second phase, however, is also in evidence which presumably consists of the additives; in addition, there is also some porosity. Under the microscope the second phase can be seen to consist of two distinct phases. Possibly corundum and hematite which have low mutual solubilities are as this second phase. The high density of billet 1255 (3.22 gm/cc (3.22 x 10$^3$ Kg/m$^3$)) is deceptive because the $Fe_2O_3$ additive clearly contributes markedly to this high value.

From previous experience in the hot pressing of materials having oxide impurities, and knowing that as well as silica being present there is some silicon present in the SiC powder, it was decided to add carbon in addition to $Al_2O_3$ to billets having high densities.

To optimize conditions, the microstructures of various billets were compared with the finest grained material (8.3 $\mu$ for billet 1233 shown in Figure 4). The structure could be considered duplex, with a small grain size material, having a tabular larger grained structure occurring with it. The grain size was measured as an average size of both the components to be 8.3 $\mu$m. The second phase is carbon, finely dispersed and not interconnected so that it will not be susceptible to removal by oxidation at high temperatures in air. In an effort, however, to reduce the carbon, billet 1237 (3 w/o

#70004                                    1500X

Figure 1.   Electron Micrograph of SiC Powder.



#5128-2                                    500X

Figure 2.   Etched Microstructure of SiC + 3 w/o $Al_2O_3$, Billet 1224.

Density 2.99 grm/cc, Grain Size 30 $\mu$.

## TABLE 1

### HOT PRESSING RESULTS OF SILICON CARBIDE

| Run No. | Additive | Grain Size μm | Temp. °F | Temp. °K | Pressure psi | Pressure N/m² x 10⁶ | Time min. | Density[1] gm/cc | Density Kg/m² x 10³ |
|---|---|---|---|---|---|---|---|---|---|
| 1209 | 3 w/o Al₂O₃ | - | 3884 | 2413 | 3000 | 20.6 | 90 | 2.8 | 2.8 |
| 1211 | 3 w/o Al₂O₃ | - | 3992 | 2473 | 3000 | 20.6 | 50 | 2.76 | 2.76 |
| 1213A* | 3 w/o Al₂O₃ 50 v/o SiC Whiskers | - | 3884 | 2413 | 3000 | 20.6 | 45 | 2.49 | 2.49 |
| 1215A | 3 w/o Al₂O₃ | - | 3884 | 2413 | 3000 | 20.6 | 120 | 2.68 | 2.68 |
| 1221A | 3 w/o Al₂O₃ 3 w/o Fe₂O₃ | - | 3884 | 2413 | 3000 | 20.6 | 60 | 2.64 | 2.64 |
| 1223A | 0 | - | 3884 | 2413 | 6000 | 41.3 | 205 | 2.89 | 2.89 |
| 1224A | 3 w/o Al₂O₃ | 30 | 3884 | 2413 | 6000 | 41.3 | 210 | 2.99 | 2.99 |
| 1225A | 3 w/o Al₂O₃ 3 w/o Fe₂O₃ | 20 | 3992 | 2473 | 6000 | 41.3 | 280 | 3.22 | 3.22 |
| 1227A | 3 w/o Al₂O₃ | - | 3992 | 2473 | 4000 | 27.5 | 210 | 2.89 | 2.89 |
| 1229 | 3 w/o Al₂O₃ | - | 3632 | 2473 | 6000 | 41.3 | Broke | | |
| 1230 | 3 w/o Al₂O₃ | - | 4064 | 2513 | 4000 | 27.5 | 210 | 2.88 | 2.88 |
| 1233 | 3 w/o Al₂O₃ 3 w/o C | 8.3 | 4064 | 2513 | 4000 | 27.5 | 210 | 3.14 | 3.14 |
| 1237 | 3 w/o Al₂O₃ | 8 | 4064 | 2513 | 4000 | 27.5 | 90 | 3.08 | 3.08 |

[1]Theoretical density of SiC = 3.21 gm/cc.

TABLE 1 (Cont'd)

HOT PRESSING RESULTS OF SILICON CARBIDE

| Run No. | Additive | Grain Size μm | Temp. °F | Temp. °K | Pressure psi | Pressure N/m² x 10⁶ | Time min. | Density gm/cc | Density Kg/m² x 10³ |
|---|---|---|---|---|---|---|---|---|---|
| 1245 | 3 w/o Al₂O₃ 1 w/o C + 50 w/o SiC Whiskers | 25 | 4064 | 2513 | 4000 | 27.5 | 150 | 2.94 | 2.94 |
| 1250 | 3 w/o Al₂O₃ 1 w/o C + 10 mats of Thornel fibers | - | 4064 | 2513 | 4000 | 27.5 | 270 | 2.86 | 2.86 |
| 1261 | 3 w/o Al₂O₃ + 1 w/o C + 25 w/o SiC Whiskers | - | 3182 | 2023 | 4000 | 27.5 | Broke before reaching temperature | | |
| 1275 | 1 w/o Al₂O₃ + 3 w/o C | 18 | 4064 | 2513 | 4000 | 27.5 | 200 | 3.19 | 3.19 |
| 1279A | 3 w/o Al₂O₃ + 1 w/o C + 25 2/o SiC Whiskers | 50 | 4064 | 2513 | 4000 | 27.5 | 200 | 2.72 | 2.72 |
| 1286 | 3 w/o Al₂O₃ + 1 w/o C + various filaments | - | 4064 | 2513 | 4000 | 27.5 | 200 | 2.8 | 2.8 |
| 1293 | 6 w/o Al₂O₃ + 3 w/o C | 45 | 4064 | 2513 | 4000 | 27.5 | 200 | 3.25 | 3.25 |
| 1316 | 3 w/o Al₂O₃ 25% SiC Whiskers, 3 w/o C | 30 large 3 small | 3632 | 2273 | 4000 | 27.5 | 220 | 3.09 | 3.09 |

## TABLE 1 (Concl'd)

### HOT PRESSING RESULTS OF SILICON CARBIDE

| Run No. | Additive | Grain Size $\mu$m | Temp. °F | Temp. °K | Pressure psi | Pressure N/m$^2$ x 10$^6$ | Time min. | Density gm/cc | Density Kg/m$^2$ x 10$^3$ |
|---|---|---|---|---|---|---|---|---|---|
| 1393 | 3 w/o Al$_2$O$_3$ + graphite cloth | - | 4064 | 2513 | 4000 | 27.5 | 255 | - | - |
| 1409 | SiC Whiskers 3% Al$_2$O$_3$ 3% C | 1 | 3632 | 2273 | 4000 | 27.5 | 205 | 3.14 | 3.14 |

* 'A' signifies 2" (5.07 x 10$^{-2}$ m) diameter billets.

No letter signifies 3" (7.61 x 10$^{-2}$ m) diameter.

## TABLE 2

### NON-DESTRUCTIVE TEST EVALUATION FOR SiC

| Billet No. | Material | Grain Size μm | Density g/cc | Density Variability % | Sonic Modulus psi x $10^6$ | | Sonic Modulus N/m2 x $10^{10}$ | |
|---|---|---|---|---|---|---|---|---|
| | | | | | Axial | Radial | Axial | Radial |
| 1245 | SiC + whiskers | 25 | 2.94 | ± 1.61 | - | - | - | - |
| 1250 | SiC + Thornel | - | 2.86 | ± 1.43 | 47.0 | - | 37.4 | - |
| 1275 | SiC | 18 | 3.19 | ± 2.54 | 62.54 | - | 43.2 | - |
| 1279A | SiC + 25% SiC Whiskers | 50 | 2.72 | ± 2.72 | 43.65 | 44.73 | 30.0 | 30.7 |
| 1286 | SiC + various filaments | - | 2.8 | ± 2.50 | 44.0 | - | 30.3 | - |
| 1293 | SiC + 6 w/o Al2O3 | 45 | 3.25 | ± 1.96 | 63.78 | - | 43.9 | - |
| 1316 | SiC + SiC Whiskers | 30 large 3.3 small | 3.09 | ± 2.1 | 50.70 | 52.53 | 34.9 | 36.0 |
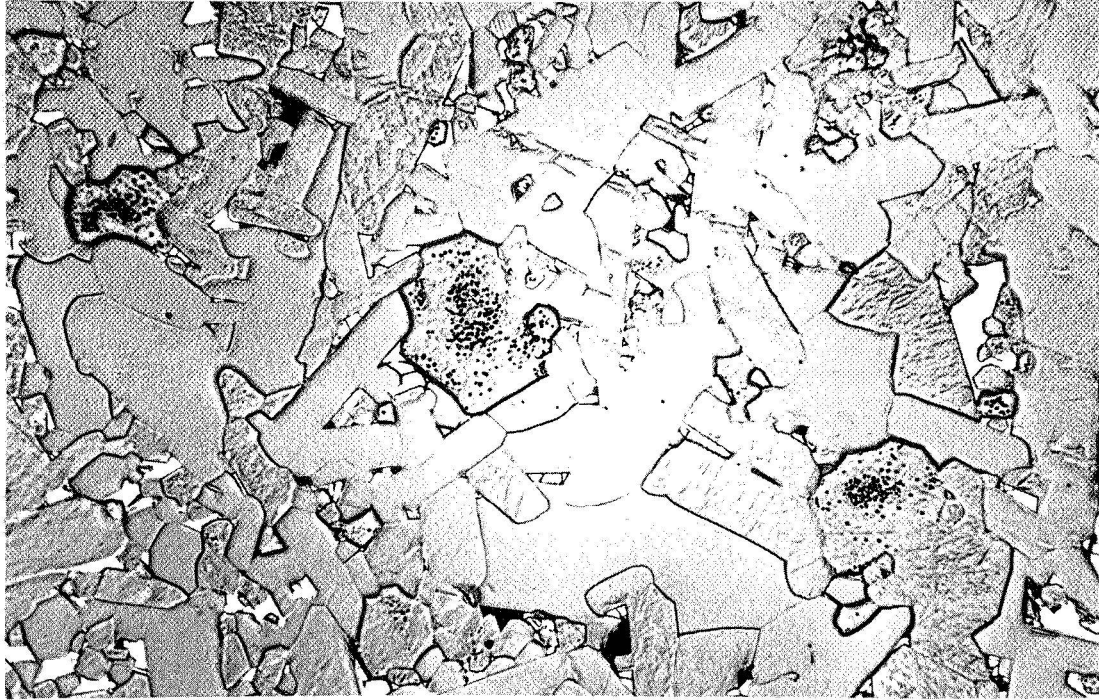
#5128-4                                                        500X

Figure 3.  Etched Microstructure of SiC with 3 w/o each of $Al_2O_3$
           and $Fe_2O_3$.  Billet 1225, Density 3.22 gm/cc, Grain
           Size 20 μ.
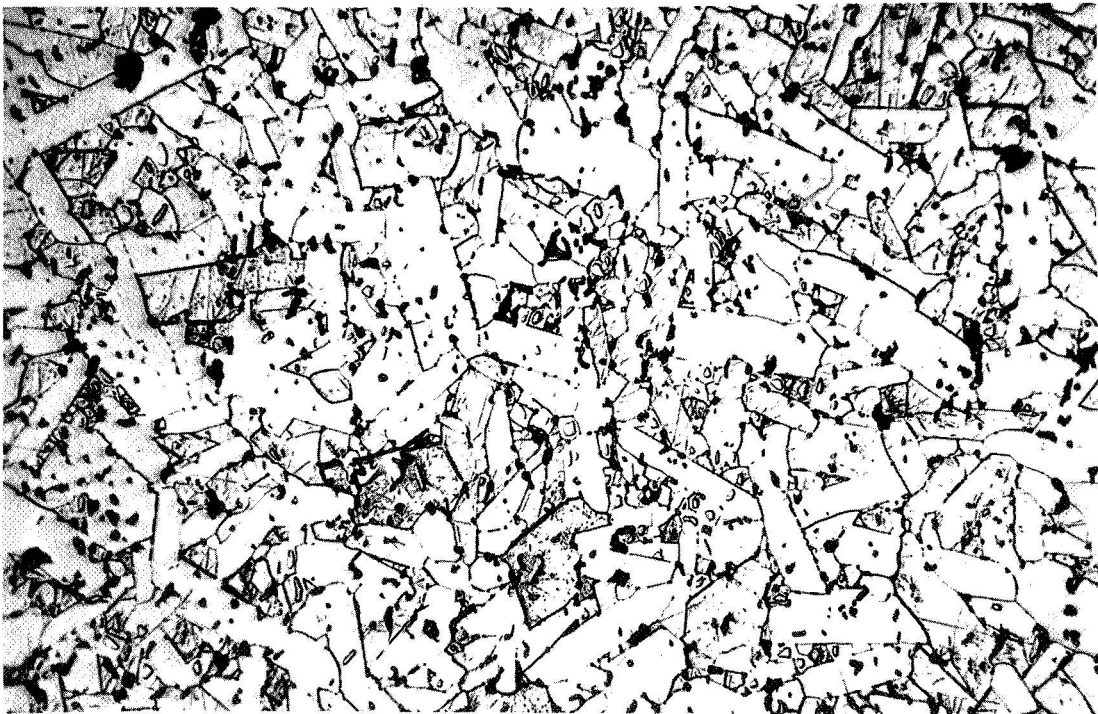


#5218-1                                                        500X

Figure 4.  Etched Microstructure of SiC with 3 w/o each of
           $Al_2O_3$ + C.  Billet 1233, Density 3.14 gm/cc, Grain
           Size 8.3 μm.

$Al_2O_3$, 1 w/o C), was prepared and is shown in Figure 5. A slightly smaller grain size than billet 1233 (Figure 4) resulted. The structure was difficult to etch and the apparent grain boundaries within each grain are artifacts. Reduction in the amount of $Al_2O_3$ in billet 1275 (1 w/o $Al_2O_3$, 3 w/o C) resulted in a microstructure shown in Figure 6. The structure is variable throughout the billet, but a point to note is that the grain size is smaller than in Figure 3, and also, the structure is no longer duplex. When even greater amounts of $Al_2O_3$ are added to SiC in billet 1293 (6 w/o $Al_2O_3$, 3 w/o C), a very large grained porous material is formed (the high measured density results from the large $Al_2O_3$ addition). The microstructure is shown in Figure 7 which shows the return of a tabular morphology with very large grain sizes and voids.

The study indicated that at the pressing condition of $4064°F$ $(2513°K)$ and 4000 psi ($27.5 \times 10^6$ N/m$^2$) a fine-grained dense SiC body can be fabricated when 3 w/o $Al_2O_3$ and from 1-3 w/o carbon is added to the SIKA grade of SiC.

### b. Filamentary Additives

Some composite structures were then prepared by adding filamentary strengthening agents to the basic SiC body. A typical view of the whiskers before adding to the powder is shown in Figure 8. After mixing the SiC whiskers in water with a Waring blender together with SiC powder, the whisker agglomerates become separated but suffer very little breakage as evidenced in Figure 9.

Figure 10 shows the resulting microstructure of a 50 v/o addition of Carborundum SiC whiskers to SiC in billet 1245. Some pull-out of some grains was unavoidable, suggesting a lower density than was the case, although a lower density body than 1237 (made with identical additives except for whiskers and under identical conditions) resulted as determined by immersion techniques ($2.94$ gm/cc, $2.94 \times 10^3$ Kg/m$^2$) no evidence of SiC whiskers was noted. When 25 v/o SiC whiskers was added to the SiC and hot pressed in billet 1279, a similar microstructure resulted, as is shown in Figure 11. It is interesting to note that there is some second phase evident at the grain boundaries, but again, no evidence of SiC whiskers as for the 50 v/o whisker addition. The billets having whiskers added have lower densities than whiskerless billets and further suffer excessive grain growth. In an attempt to preserve the whisker morphology, a SiC body with 25 v/o SiC whiskers added (billet 1316) was pressed at a lower temperature than that required for complete densification of that structure ($3632°F$ ($2274°K$) instead of $4064°F$ ($2513°K$). It should be noted, however, that the density obtained ($3.09$ gm/cc, $3.09 \times 10^3$ Kg/m$^2$ was higher than similar pressings having whisker additives when pressed at $4064°F$ ($2513°K$).

If whiskers are present in SiC powder at temperatures required to consolidate pure SiC, then they presumably act as nucleation sites in the growth of large grains with the $Al_2O_3$ additives providing a mechanism for the process. At slightly lower temperatures high densities can be obtained (although not full density) without the attendant grain growth of the matrix. The kinetics of the SiC phase change from $\beta \longrightarrow \alpha$ during densification may be the key to the process.
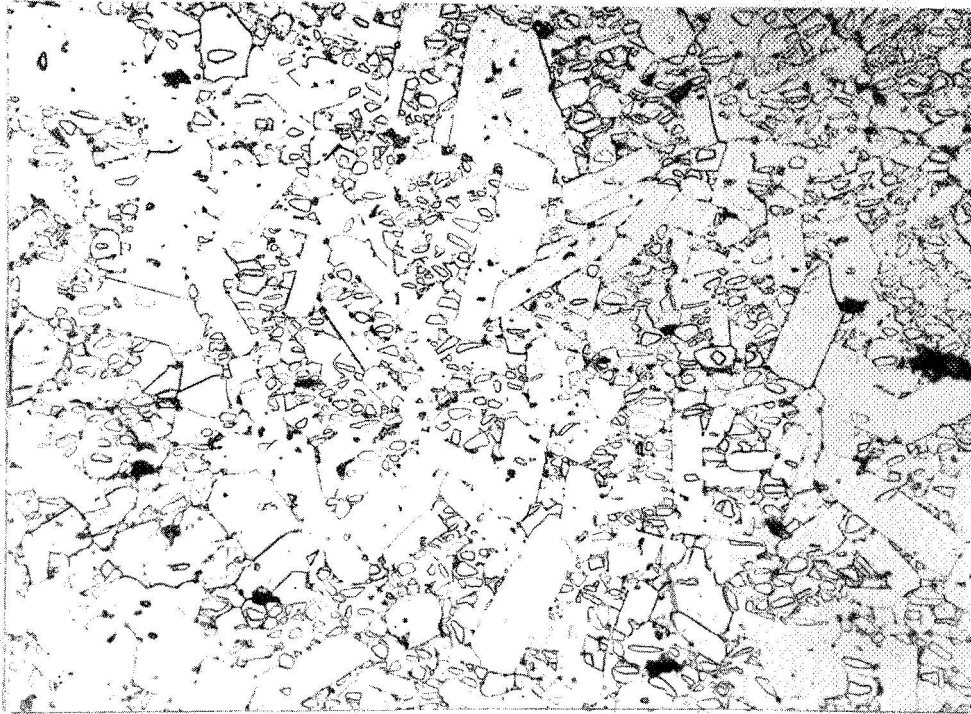
#5138                                                    500X

Figure 5.   Etched Structure of SiC with 3 w/o Al₂O₃ and 1 w/o C.
            Billet 1237, Density 3.08 gm/cc, Grain Size 8 μ.



#5187                                                    500X

Figure 6.   Etched Microstructure of SiC with 1 w/o Al₂O₃ and
            3 w/o C.   Billet 1275, Density 3.19 gm/cc, Grain
            Size 18 μ.
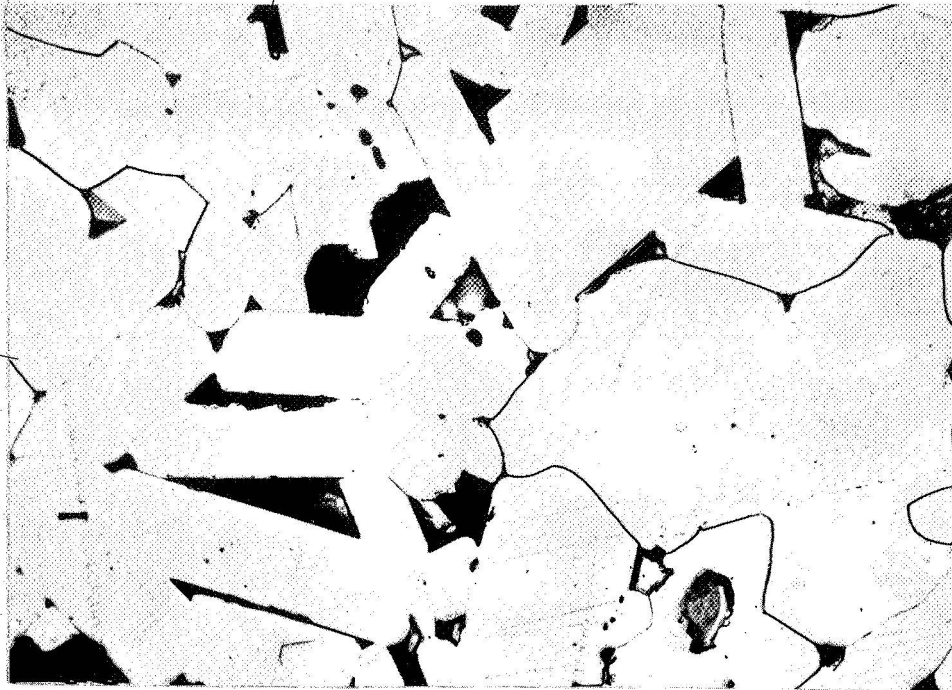
#5200-3                                                    500X

Figure 7.   Etched Microstructure of SiC with 1 w/o $Al_2O_3$ and
            3 w/o C.  Billet 1293, Density 3.25 gm/cc, Grain
            Size 45 μ.
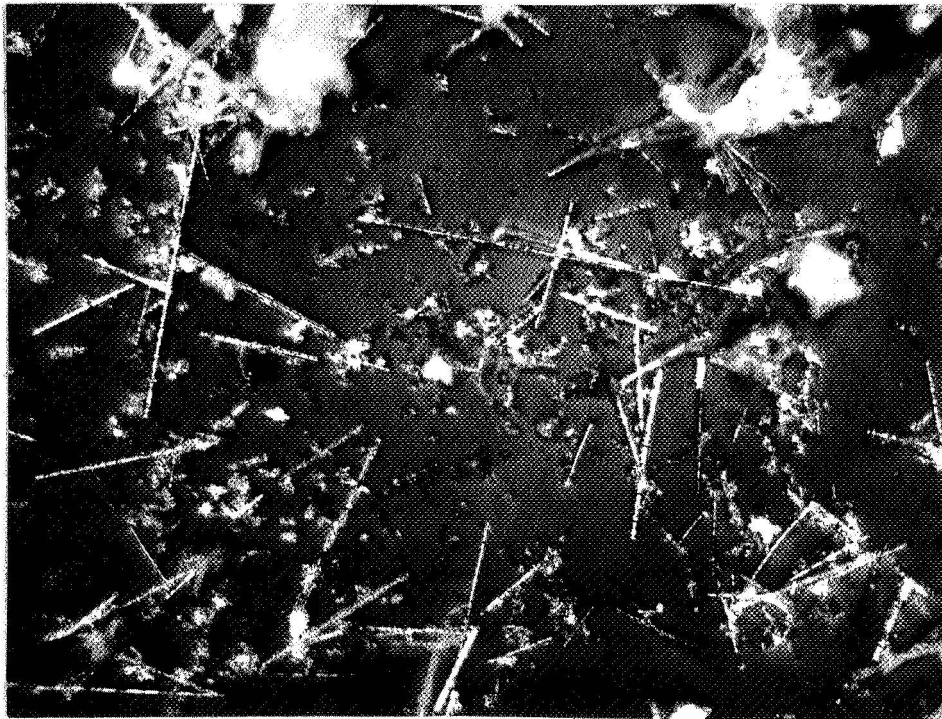


#5099-2                                                    500X

Figure 8.   SiC Whiskers (approximately 1 μm diameter).

## TABLE 3

### SUMMARY OF SiC PRESSINGS WITH VARYING AMOUNTS

### OF ALUMINA AND CARBON ADDITIVES

| Billet No. | Density gm/cc | Kg/m² x 10³ Density | $Al_2O_3$ Addition w/o | C Addition w/o | Grain Size $\mu$m |
|---|---|---|---|---|---|
| 1233 | 3.14 | 3.14 | 3 | 3 | 8.3 |
| 1237 | 3.08 | 3.08 | 3 | 1 | 8.0 |
| 1275 | 3.19 | 3.19 | 1 | 3 | 18 |
| 1293 | 3.25 | 3.25 | 6 | 3 | 45 |
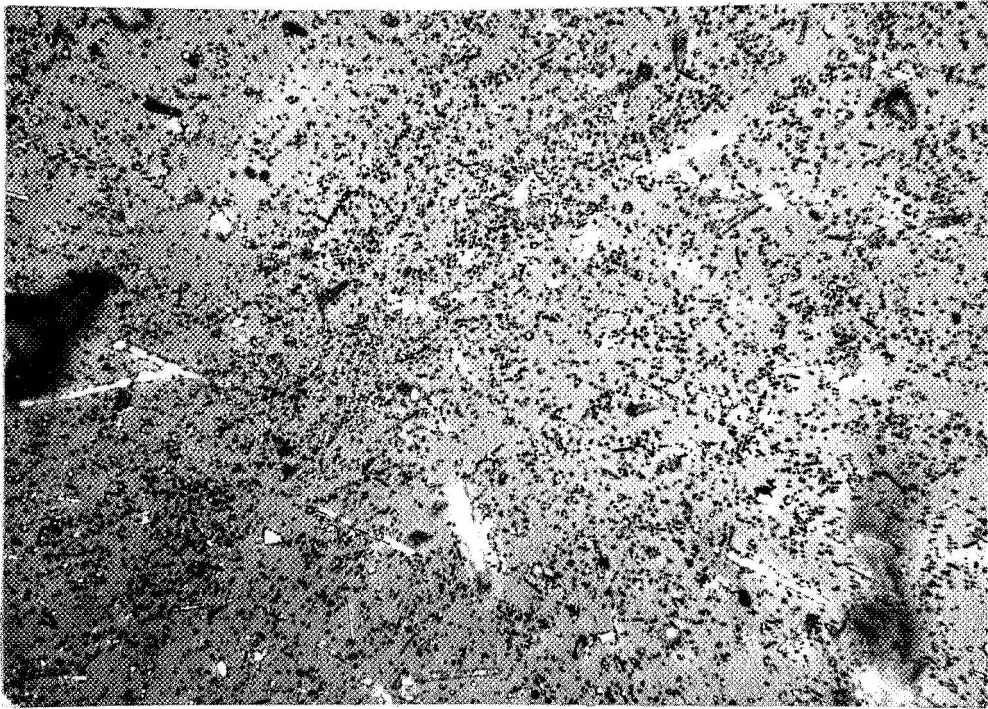
#5099-1                                                              500X

Figure 9.  SiC Whiskers after Mixing with SiC Powder.
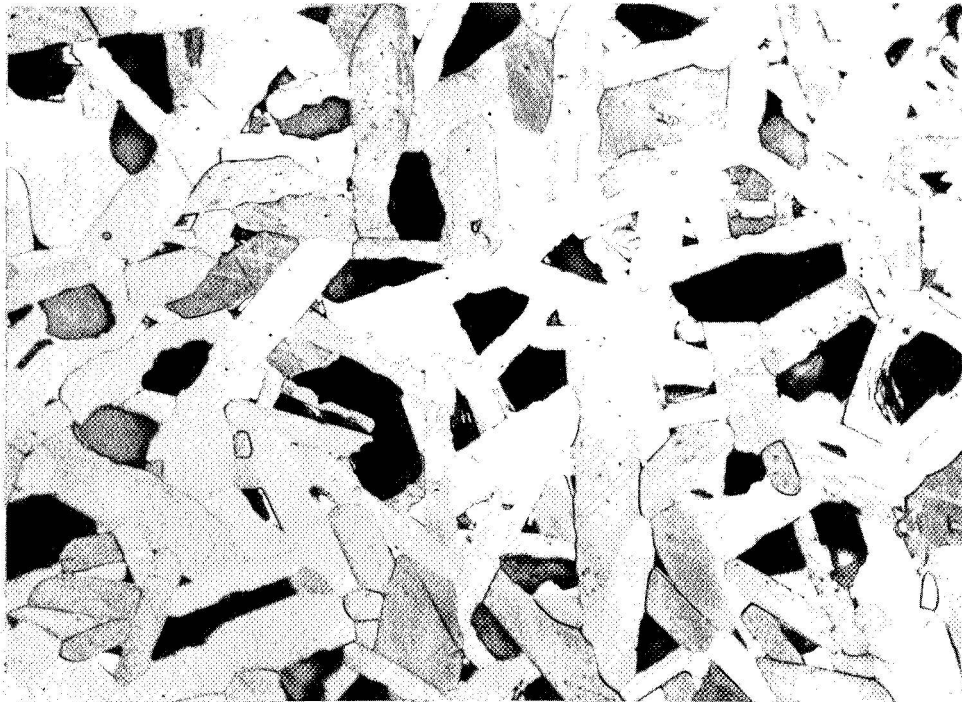


#5162-1                                                              500X

Figure 10.  Etched Microstructure of SiC with 50 v/o SiC
            Whiskers Added.  Billet 1245, Density 2.94 gm/cc,
            Grain Size 25 μ.
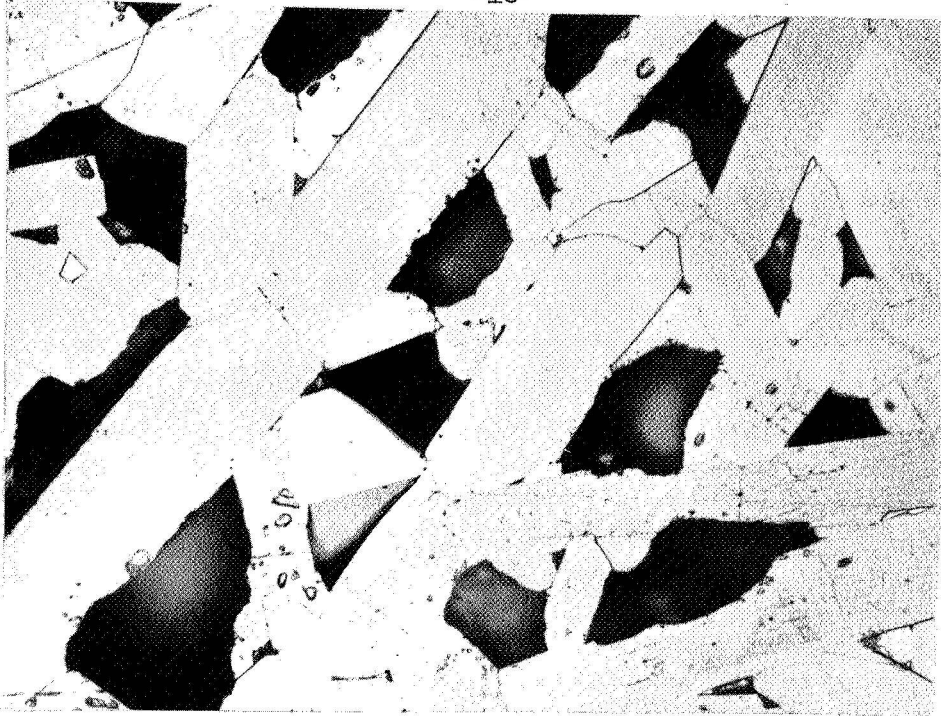
#5198                                                     500X

Figure 11.   Etched Microstructure of SiC with 25 v/o SiC
             Whiskers.  Billet 1279, Density 2.72 gm/cc, Grain
             Size 50 μ.
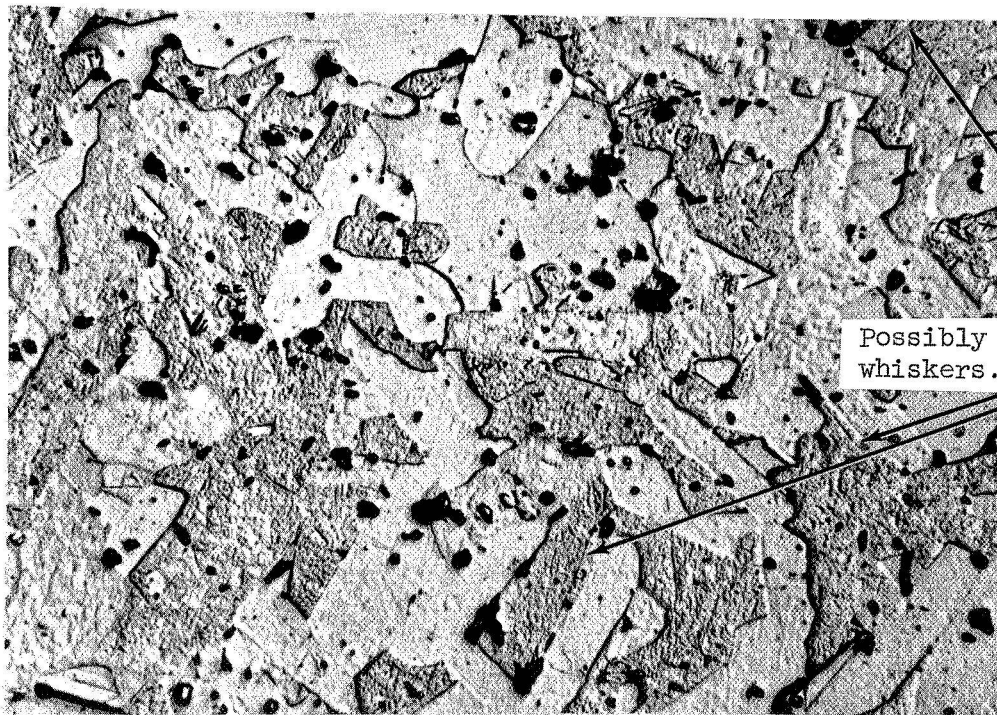


Possibly retained
whiskers.

#5231-1                                                   500X

Figure 12.   Etched Microstructure of SiC with 3 w/o Al$_2$O$_3$,
             3 w/o C and 25 w/o SiC Whiskers.  Billet 1316,
             Density 3.09 gm/cc, Grain Size 30 μ.

Metallographic examination of the SiC whisker added to SiC (billet 1316) was made and the structure is shown in Figure 12. Although the retention of SiC whiskers cannot be seen specifically, there are long fine structures at grain boundaries in many parts of the billet which may be retained whiskers.

The remnants of the SiC whiskers were pressed into a billet with 3% $Al_2O_3$ and 3% carbon additions (billet 1409). Metallography showed a fibrous-like structure barely resolvable using an oil immersion objective. Replicas of the fractured surface did not show this fibrous pattern but indicated a fine-grained structure of approximately 1 μm, but with no traces of whiskers in evidence. The fracture obtained during impact testing was of transgranular nature as found before for SiC but the grains showed a very high evidence of parallel steps in the fracture path.

### c. Other Additives

To investigate the potential of other commercially available filaments, a billet 1286 was prepared in which the following candidate filaments were placed in a plane at the center of a SiC billet:

| Fiber | Source |
|---|---|
| Boron carbide yarn | Beaunit Fibers |
| Carbon monofilament | Great Lakes Carbon Corp. |
| SiC on W substrate mono-<br>filament | Dow Chemical |
| Single crystal sapphire<br>filament | Tyco |
| SiC whiskers | Carborundum |
| Thornel yarn | Union Carbide |

As with other billets where filamentary additives have been made, a low density of 2.8 gm/cc ($2.8 \times 10^3$ $Kg/m^2$) was obtained. Microstructural examination of the billet revealed no recognizable trace of any of the filamentary additives. It appears that at 4064°F (2513°K) pressing temperature, none of the fibers currently available which show promise as strengthening materials can survive except for Thornel filament. By analogy with the whisker additions to SiC, a lower hot pressing temperature, although 100% density cannot be attained, may be the solution if fiber morphology is to be retained.

A composite structure based on SiC was prepared using mats of Thornel filaments, pre-impregnated with a water slurry of SiC powder. The resultant billet 1250 was examined metallographically which indicated that the slurry technique resulted in penetration of the Thornel yarn by SiC but was not complete. The middle layers of SiC matrix were substantially less dense than the surface layers. Although the feature itself is undesirable, it does suggest a composite behavior at high temperature during pressing, because of stress transfer to the Thornel fiber mats which reduced the stress available at the center of the billet below that necessary for consolidation. A typical microstructure along the length of one piece of Thornel yarn is shown in Figure 13a and across the fiber in Figure 13b. Nondestructive radiography indicated that the mats were equally spaced after pressing.

#5197                                                        500X

Figure 13a.   Etched Microstructure of SiC Showing a Thornel
              Fiber in the Longitudinal Direction.   Billet 1250
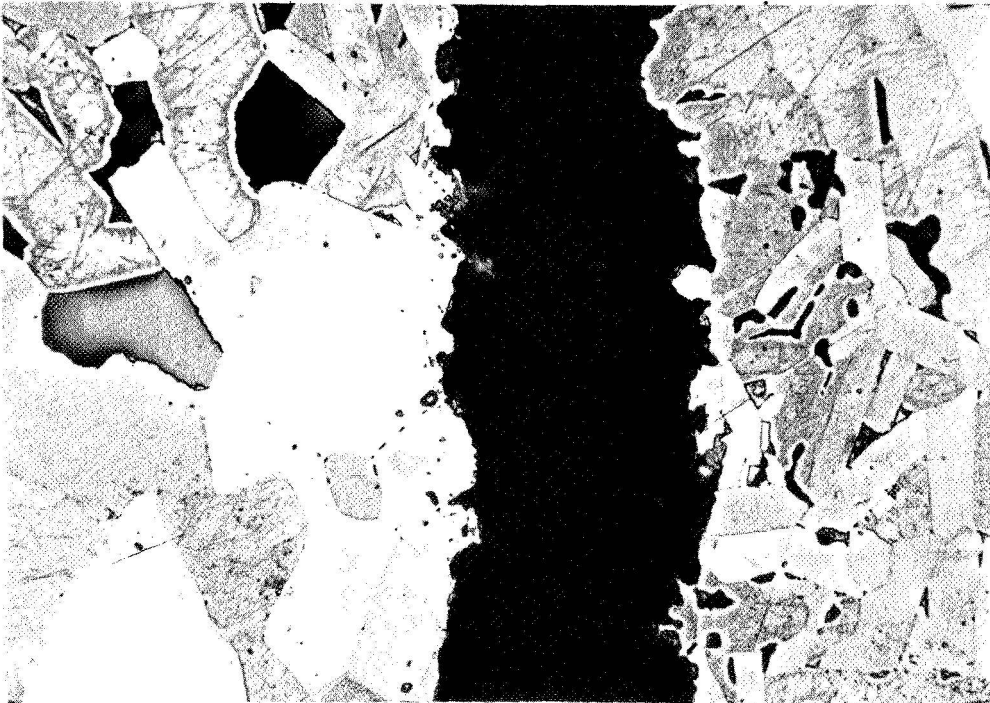


#5197-1                                                      500X

Figure 13b.   Etched Microstructure of SiC Showing Cross-Section
              of Thornel Fiber.   Billet 1250

B. **Silicon Nitride Fabrication**

1. **Powder Characterization**

Apart from billet 1401, all the 3-inch (7.92 x $10^{-2}$ m) diameter pressings of $Si_3N_4$ have been made exclusively from the powder obtained from Shieldalloy, who are agents for Hermann C. Starck of Berlin, Germany. The analysis given was quoted to be

> N - 39.02%
> Si - 61.10%
> C - 0.05%

with a particle size of -325 mesh.

Analysis made using x-ray diffraction and comparing with standard powder samples specially prepared for the purpose gave the following results:

| Major constituent - | $-Si_3N_4$ |
|---|---|
| Minor | Si |
| Minor | $-Si_3N_4$ |
| Trace | $Si_2ON_2$ |

The free silicon was estimated to be 1-2% based on comparison of the peak area ratios (Si(111)/$\beta$-$Si_3N_4$ (200) of the sample and two standards. No SiC or $SiO_2$ was detected. Metallography of the powder showed silicon to be present as discrete particles usually at the large end of the size distribution. Electron microscope examination showed a distribution of sizes from 0.1 um to 40 um, Figure 14. No distribution of sizes was determined but the powder clearly consisted of all those particles which passed through a 325 mesh sieve. A polished section mounted in epoxy resin clearly showed a second phase both separately and in conjunction with the $Si_3N_4$ found in the x-ray analysis and not silicon since it cannot be removed by HF.

Powder containing 85% $\alpha$-$Si_3N_4$ was obtained from Royal Doulton in the U.K. via Materials Research Corporation at the end of the program after long delays. X-ray diffraction confirmed the $\alpha/\beta$ ratio in the powder. However, little more characterization of this powder was made.

2. **Hot Pressing**

The conditions for all the silicon nitride billets prepared are shown in Table 4 and their NDT results in Table 5.

a. **Densification Additives**

By analogy with the experience gained in hot pressing SiC, 2 w/o graphite was added to account for the silicon impurity present and to convert this to SiC. According to the work of Deeley,[7] a5% addition of MgO

#69871A                                                    1500X

Figure 14.   Electron Micrograph of Si₃N₄ Powder.



Gold
colored
phase
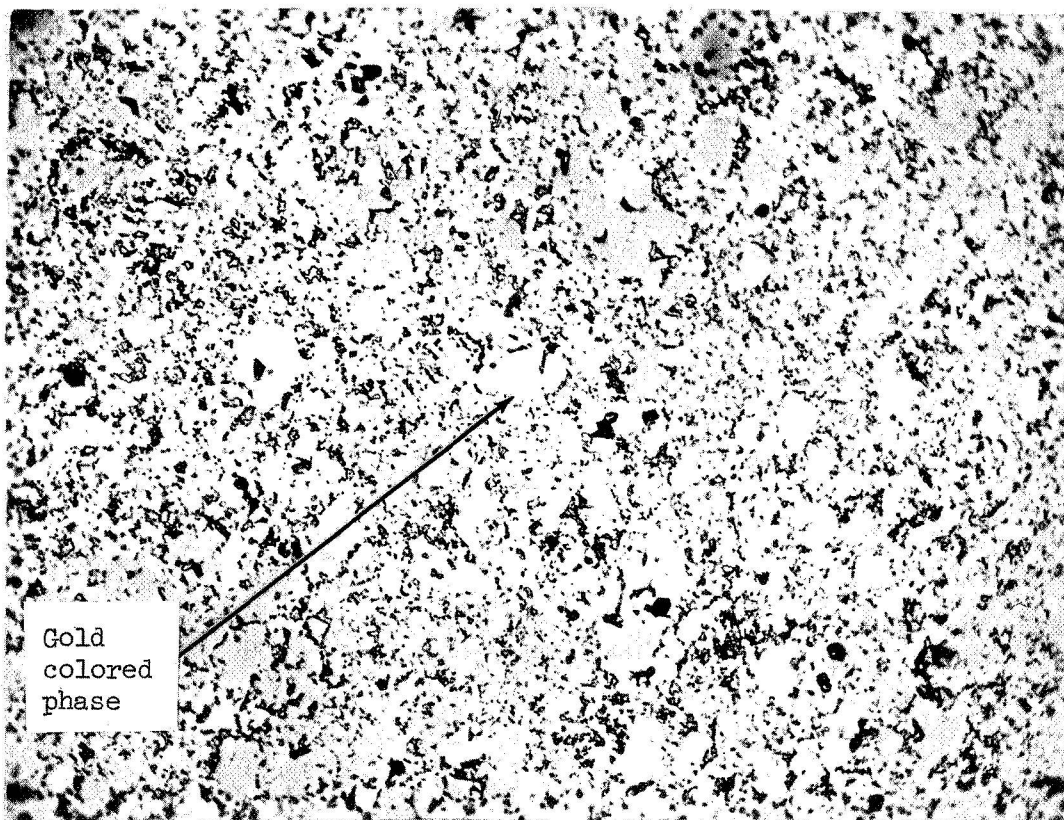
#5163                                                      500X

Figure 15.   Polished Section of Si₃N₄ with 5 w/o MgO and 2 w/o C.
             Billet 1249, Density 3.2 gm/cc, Grain Size unknown.

TABLE 4

HOT PRESSING RESULTS OF SILICON NITRIDE

| Run No. | Additive | Grain Size $\mu m$ | Temp. °F | Temp. °K | Pressure psi | Pressure $N/m^2$ x $10^6$ | Time min. | Density[1] gm/cc | Density $Kg/m^2$ x $10^3$ |
|---|---|---|---|---|---|---|---|---|---|
| 1367* | 5 w/o MgO | - | 3272 | 2073 | 5000 | 34.5 | 15 | 3.18 | 3.18 |
| 1370* | 5 w/o MgO | - | 3272 | 1873 | 1000 | 6.89 | 30 | 2.16 | 2.16 |
| 1381* | Repressed with ZrO₂ | - | 3272 | 2073 | 5000 | 34.5 | 98 | 3.50 | 3.50 |
| 1249A+ | 5 w/o MgO 2 w/o C | - | 3272 | 2073 | 4000 | 27.5 | 53 | 3.20 | 3.20 |
| 1251 | 5 w/o MgO + 2 w/o C | 2.5 | 3272 | 2073 | 4000 | 27.5 | 270 | 3.19 | 3.19 |
| 1262 | 5 w/o MgO + 2 w/o C 25 w/o SiC Whiskers | 1 | 3272 | 2073 | 4000 | 27.5 | 120 | 3.18 | 3.18 |
| 1281 | 5 w/o MgO + 2 w/o C 10 Thornel mats | - | 3272 | 2703 | 4000 | 27.5 | 100 | 3.15 | 3.15 |
| 1289 | 5 w/o MgO + 2 w/o C + various filaments | - | 3272 | 2073 | 4000 | 27.5 |  | 3.21 | 3.21 |
| 1319 | 5 w/o MgO | 1.75 | 3272 | 2703 | 4000 | 27.5 | 60 | 3.19 | 3.19 |
| 1336 | 5 w/o MgO + 2 w/o C + SiC monofilaments | - | 3272 | 2703 | 4000 | 27.5 | 90 | 3.18 | 3.18 |
| 1377 | 5 w/o MgO + W, Mo, Re, SiC Whiskers | - | 3272 | 2703 | 4000 | 27.5 | 210 | - | - |
| 1397 | 5 w/o MgO + 2 w/o C + Mo wires | - | 3272 | 2703 | 4000 | 27.5 | 105 | 3.36 | 3.36 |

[1]Theoretical density of $Si_3N_4$ = 3.19 gm/cc.

## TABLE 4 (Concl'd)

### HOT PRESSING RESULTS OF SILICON NITRIDE

| Run No. | Additive | Grain Size μm | Temp. °F | Temp. °K | Pressure psi | Pressure N/m² x 10⁶ | Time min. | Density gm/cc | Density Kg/m² x 10³ |
|---|---|---|---|---|---|---|---|---|---|
| 1401† | 5 MgO (85% α-Si₃N₄) | 0.77 | 3092 | 1973 | 4000 | 27.5 | 80 | | |
| | | | 3182 | 2023 | 4000 | 27.5 | 90 | | 3.20 |
| | | | 3182 | 2023 | 4000 | 27.5 · | 100 | 3.20 | |
| 1407 | 5 w/o MgAl₂O₄ 2 w/o C | 0.62 | 3272 | 2703 | 4000 | 27.5 | 93 | 3.24 | 3.24 |

\* 1/2" (1.27 x 10⁻² m) diameter trial pressings.

⁺A signifies 2" (5.08 x 10⁻² m) diameter pressing.

† 85 v/o α-Si₃N₄ Royal Doulton powder used.

TABLE 5

NON-DESTRUCTIVE TEST EVALUATIONS FOR SILICON NITRIDE

| Billet No. | Material | Grain Size μm | Density gm/cc | Density Variability % | Sonic Modulus psi x 10$^6$ | | Sonic Modulus N/m$^2$ x 10$^{10}$ | |
|---|---|---|---|---|---|---|---|---|
| | | | | | Axial | Radial | Axial | Radial |
| 1251 | Si$_3$N$_4$ | 2.5 | 3.19 | ± 1.1 | - | - | - | - |
| 1262 | Si$_3$N$_4$ + SiC Whiskers (before grinding off skin) | 1 | 3.07 | ± 2.45 | - | - | - | - |
| 1262 | Si$_3$N$_4$ + SiC Whiskers (after grinding off skin) | 1 | 3.07 | ± 2.45 | 52.18 | 58.17 | 36.4 | 40.0 |
| 1281 | Si$_3$N$_4$ + Thornel mats | - | 3.15 | ± 2.38 | Not possible | | Not possible | |
| 1289 | Si$_3$N$_4$ + various filaments | - | 3.21 | ± 0.73 | 55.33 | - | 48.1 | - |
| 1319 | Si$_3$N$_4$ + 5 w/o MgO | 1.75 | 3.19 | ± 0.63 | 40.61 | 43.10 | 28.0 | 29.7 |
| 1336 | Si$_3$N$_4$ + SiC filaments | - | 3.19 | ± 2.4 | 41.4 | 42.78 | 28.5 | 29.5 |

acts as a 'flux' and facilitates the densification of $Si_3N_4$ when hot pressing at $3362°F$ ($2123°K$) to give bodies having less than 0.1% porosity. This amount of MgO was added in addition to the carbon and dense billets of $Si_3N_4$ have been successfully prepared (see Table 4). A microstructure of billet 1249 is shown in Figure 15. Apart from the graphite phase there is a light colored impurity phase present in the center of Figure 15, but which shows as golden copper colored when seen in the microscope. The material is birefringent as opposed to the matrix which is not optically active. It has been reported[8] that $\alpha$-$Si_3N_4$ is birefringent and is also mechanically harder than the high temperature $\beta$-$Si_3N_4$. Microhardness measurements, however, show the second phase to be substantially softer than the matrix. X-ray diffraction on a polished surface shows no $\alpha$-$Si_3N_4$ but a pattern which could be identified either as SiC, $MgSiN_2$ or $Mg_2SiO_4$ (essentially similar patterns with respect to the 3 most intense lines) -- the microhardness measurements preclude the presence of SiC although this phase may be present in smaller quantities elsewhere in the structure as the product of the reaction between the silicon impurity and the carbon additive. Using a 200 gm load, the average microhardness of the $Si_3N_4$ matrix is 1391 $Kg/mm^2$ ($1.3 \times 10^6$ $N/m^2$) Knoop and the golden phase 884 $Kg/mm^2$ ($8.66 \times 10^4$ $N/m^2$) Knoop. The x-ray analysis did not show Si, $\alpha$-$Si_3N_4$, $SiO_2$, $Si_2ON_4$, MgO, magnesium carbides, $Mg_3N_2$ or $Mg_2Si$. The phase is not removed by concentrated or dilute nitric acid, cold HF, aqua regia, but is removed by hot HF after 1 hour and rapidly by $HF/HNO_3$.

The etching of $Si_3N_4$ to reveal the grain structure proved difficult and the following techniques have been used without success:

$HF/HNO_3$ mixture cold
Flame tinting
Phosphoric acid at $400°F$ ($447°K$) for 1 hour
Thermal etching in vacuum at $1832°F$ ($1273°K$) for 1 hour

The thermally etched specimen after lightly repolishing, indicates some very fine structure, but is not suitable for grain size measurements.

A $Si_3N_4$ billet (1319) having a 5 w/o MgO addition but no carbon addition was examined both metallographically and also by replication of a fractured surface in the electron microscope. Optically, there appears to be more gold-colored second phase and light grey phase present than when carbon is added. Figure 16 shows a typical area of the section; the "arrowed" very light second phase is the gold-colored material. Replicas were taken from a fractured surface and the grain size measured as 2.5 $\mu$m. Various portions of the surface are shown in Figure 17a and b and some of the surface of the $Si_3N_4$ billet 1319 which was pulled out during replication was analyzed using electron diffraction. From the large size of these pull-outs compared with the $Si_3N_4$ grain size, they are thought to have derived from the gold phase. The diffraction patterns were analyzed to be mainly $\beta$-$Si_3N_4$ with 2 reflections similar to the one found by x-ray diffraction.

The precise identification of the gold phase found in hot pressed $Si_3N_4$ employing an MgO densification aid is, therefore, ambiguous. It should be noted that in their study on the mechanism of MgO in the hot
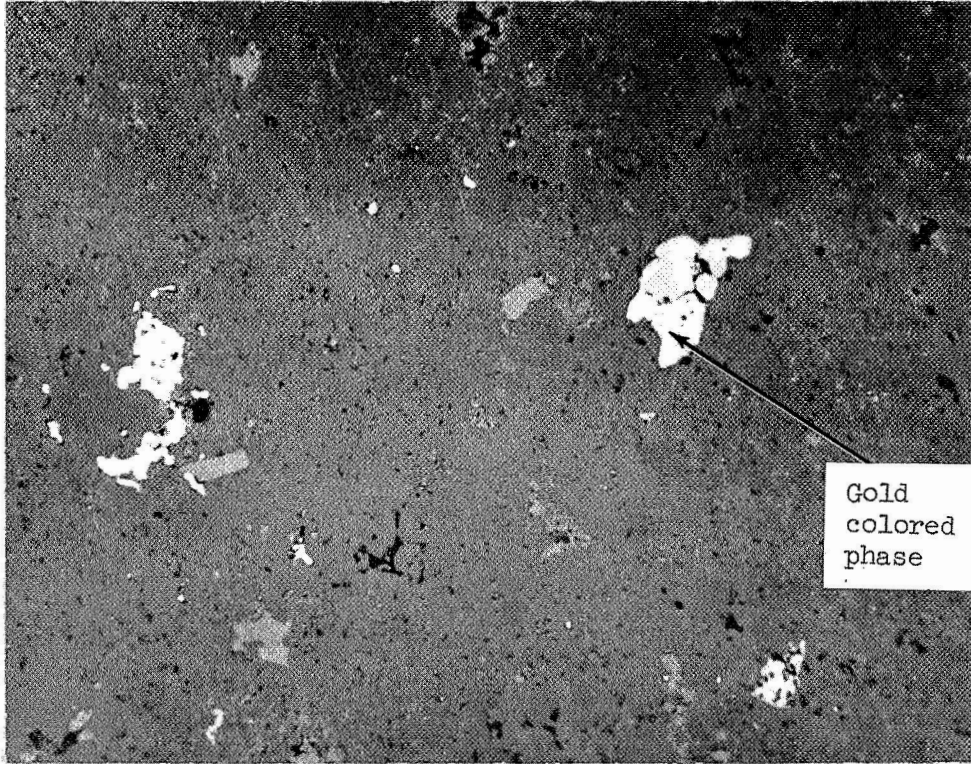
#5231                                                        500X

Figure 16.    Polished Section of Si₃N₄ with 5 w/o MgO.
              Billet 1319, Density 3.19 gm/cc, Grain Size 1.75 μ.

#70183　　　　　　　　　　　　(a)　　　　　　　　　　　　2000X



#70185　　　　　　　　　　　　(b)　　　　　　　　　　　　7500X

Figure 17.　Fractograph of Si₃N₄ with 5 w/o MgO.　Billet 1319,
Density 3.19 gm/cc, Grain Size 1.75 μ.

pressing of $Si_3N_4$, Grieveson[14] reports that they identified quantitatively the presence of $Mg_2SiO_4$ in hot pressed $Si_3N_4$. No indication was given by the authors as to the total number of reflections used for the identification; only three forsterite reflections ("d" $\sim$ 2.7, 2.5 and 2.4 Å) are reported and it is interesting to note that these same three spacings also correspond to the three strongest lines for $MgSiN_2$ ("d" = 2.75, 2.49 and 2.41 Å), respectively, and that similar lines were obtained in the x-ray analysis of billet 1249 performed in this laboratory.

In the replica of the fractured surface of billet 1319, there is clearly a grain boundary phase present seen best in Figure 17b at the boundaries and as a rough area on the surface of some grains. There is some very fine particulate structure present particularly in Figure 17b, but very much less than that found in $Si_3N_4$ when carbon is added. A fractograph of such a material taken from billet 1251 is shown in Figure 18. The finer grain size is evident (1.91 μm average) as also is a large quantity of very fine particulate structure. The carbon which is added prior to pressing is Regal 330R graphite which has an average particle size of 250 Å, (2.5 x $10^{-8}$ m). It is added to convert any silicon or $SiO_2$ impurities to SiC, since this reaction may take place at temperatures lower than the 3272°F (2073°K) used for $Si_3N_4$ pressing temperatures. A plot of free energy of formation versus temperature in Figure 19 indicates that carbon will react with $Si_3N_4$ to form nitrogen and SiC above 2776°F (1798°K) at 1 atmosphere pressure (1.01 x $10^5$ N/m²). Although the applied pressure of 4000 psi (27.5 x $10^6$ N/m²) used during hot pressing will increase this temperature somewhat, any residual carbon will react with $Si_3N_4$ at 3272°F (2073°K) forming SiC. The small particles in Figure 18 are, therefore, thought to consist mainly of SiC.

Outstanding properties for $Si_3N_4$ have been reported[13] when powder containing a very high proportion of the low temperature $\alpha$-$Si_3N_4$ is pressed. A fine grain material results having exceptional mechanical properties, e.g., a modulus of rupture in excess of 100,000 psi (6.89 x $10^8$ N/m²) at room temperature. The material was pressed following the conditions reported by Lumby[13] using powder obtained from Royal Doulton which contained 85% $\alpha$-$Si_3N_4$ and a dense billet 1401 resulted. A grain size of 0.77 μm average was determined by replication of a fractured surface. The value is double that reported,[13] but nonetheless, lower than the value found for billets pressed from essentially all $\beta$-$Si_3N_4$, (c.f., billet 1319 - 2.5 μm, billet 1251 - 1.19 μm). Until recently the $\alpha$-$Si_3N_4$ was thought to be a low temperature form of $Si_3N_4$. However, work by Grieveson[14] et al, has shown that $\alpha$-$Si_3N_4$ is $Si_{11.5}N_{15}O_{0.5}$ which is formed above a certain oxygen potential in the gas phase of $NH_3$-$H_2$ mixture on reaction with silicon. It is also shown that the MgO used as an additive in hot pressing formed a magnesium silicate of composition near enstatite ($MgSiO_3$) to provide a flux for densification while the '$\alpha$-$Si_3N_4$' to $\beta$-$Si_3N_4$ provides a mechanism for grain refinement. The retention of a glassy phase of $MgSiO_3$, however, may result in a rapid loss of strength at high temperatures particularly if it is retained at the grain boundaries as a discrete phase.

A billet (1407) was prepared using spinel ($MgAl_2O_4$ as additive Table 4). Good densification was achieved and also the grain size measured as 0.62 μm was the lowest obtained in this work. This material is shown as a fractograph in Figure 20.

#70054                                                    7500X

Figure 18.   Fractograph of $Si_3N_4$ with 5 w/o MgO + 2 w/o C.
             Billet 1251, Density 3.19 gm/cc, Grain Size 1.91 $\mu$
             Average, 0.2 $\mu$, Smallest Observed.

Figure 19. Standard Free Energies of Formation of Some Nitrides
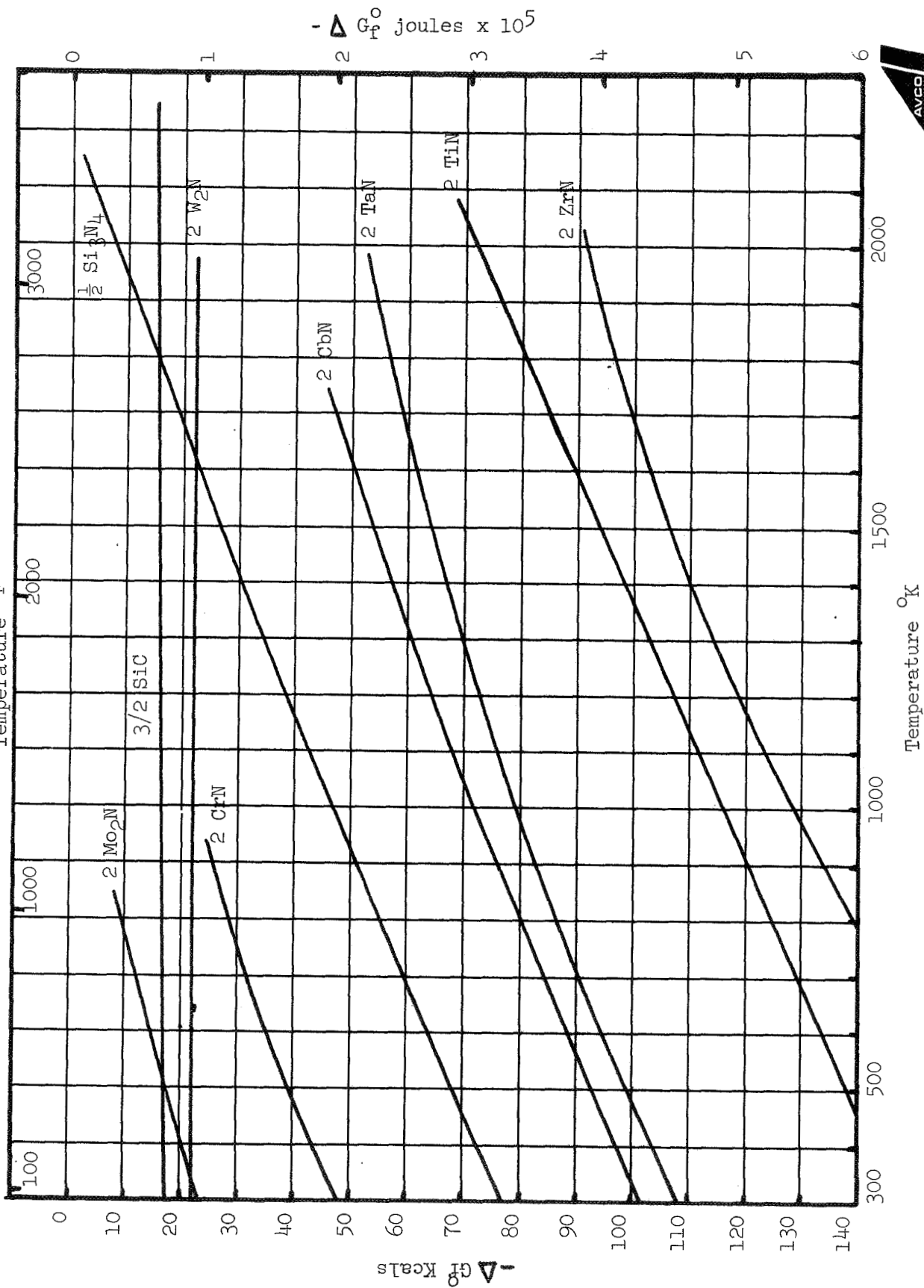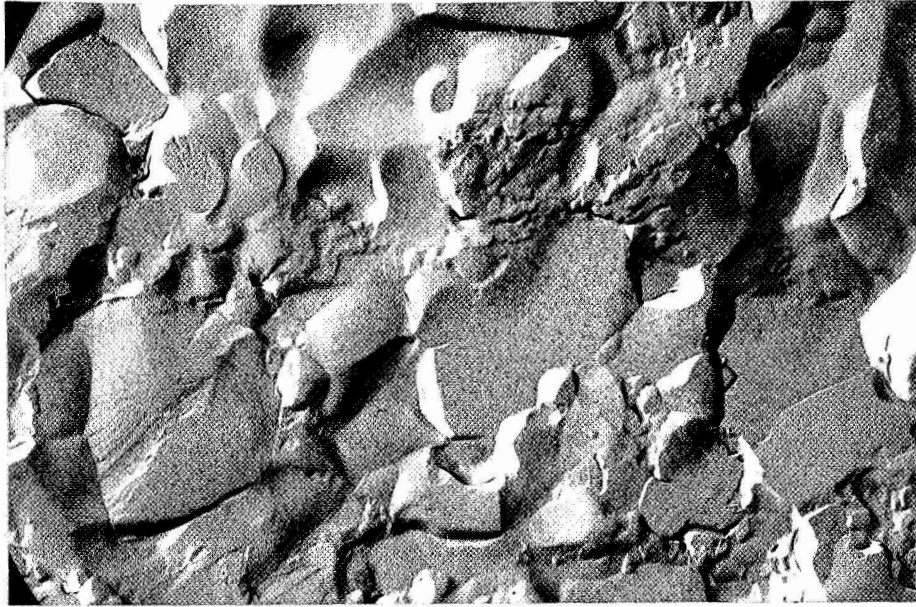
#70454                                                    15,000X

Figure 20.   Fractograph of Si3N4 with 5 w/o MgAl2O4.  Billet
             1407, Density 3.24 gm/cc, Grain Size 0.62 μ.

### b. Filamentary Additives

As shown in Table 4, a billet 1262 containing 25 w/o SiC whiskers was successfully fabricated and was used for further testing. Although the density was 97% of theoretical, the sonic modulus was higher than for $Si_3N_4$ having no whisker additive, (c.f., billet 1262 and 1319 in NDT results, Table 5). This was an indication that the whiskers were contributing to the mechanical properties of the composite. The discussion regarding the retention of whisker morphology is presented in Section IV.D.4 where fractographs of the samples are presented.

### c. Other Additives

A composite billet 1281 made from $Si_3N_4$ and ten Thornel mats was made in an analogous manner to the SiC billet 1250. Although the matrix densified satisfactorily, some of the Thornel layers became bloated. Possibly the following reaction was responsible for this separation - working against a pressure applied during hot pressing of 4000 psi ($27.5 \times 10^6$ $N/m^2$):

$$Si_3N_4 + 3C \longrightarrow 3 SiC + 2N_2 \quad \Delta G^o = 34.76 \text{ Kcals} \qquad (1)$$
$$(1.43 \times 10^5 \text{ J}) \text{ at } 3130^oF \ (2000^oK)$$
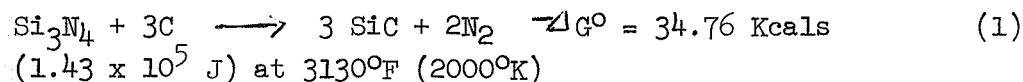
with free energy computed from the JANAF tables.

Thus, a nitrogen equilibrium pressure of nearly 12,000 psi ($8.29 \times 10^7$ $N/m^2$) is developed. There was a skin around the billet 1281 of faint green tint and this same material appears to be associated with the Thornel filaments too. This coating is suggestive of SiC and has been confirmed as such metallographically. Thus, for some layers, their edges became sealed by reaction between the $Si_3N_4$ matrix and the carbon die liner and the nitrogen evolved as a result of Eq. (1) causes bloating in those regions. Judicious selection of release agents such as boron nitride allow the $Si_3N_4$ to be fabricated in graphite die materials.

A billet (1289) containing experimental filaments as described for SiC billet 1286 was prepared using $Si_3N_4$. These filaments were as before:

| Fiber | Source |
|---|---|
| Boron carbide | Beaunit Fibers |
| Carbon monofilament | Great Lakes Carbon Corp. |
| SiC on W substrate mono-filament | Dow Chemical |
| Single crystal sapphire filament | Tyco |
| SiC whiskers | Carborundum |
| Thornel yarn | Union Carbide |

The billet (1289) was sectioned and analyzed metallographically. The $B_4C$ filament was made by Beaunit by extruded cellulose acetate fibers loaded with 25 v/o $B_4C$ powder. The organic portion was shown to have decomposed during hot pressing leaving behind little $B_4C$ which could be useful. Figure 21 shows three strands of carbon monofilament. Surrounding each is a reaction zone consisting of SiC. Figure 22 shows a SiC monofilament in
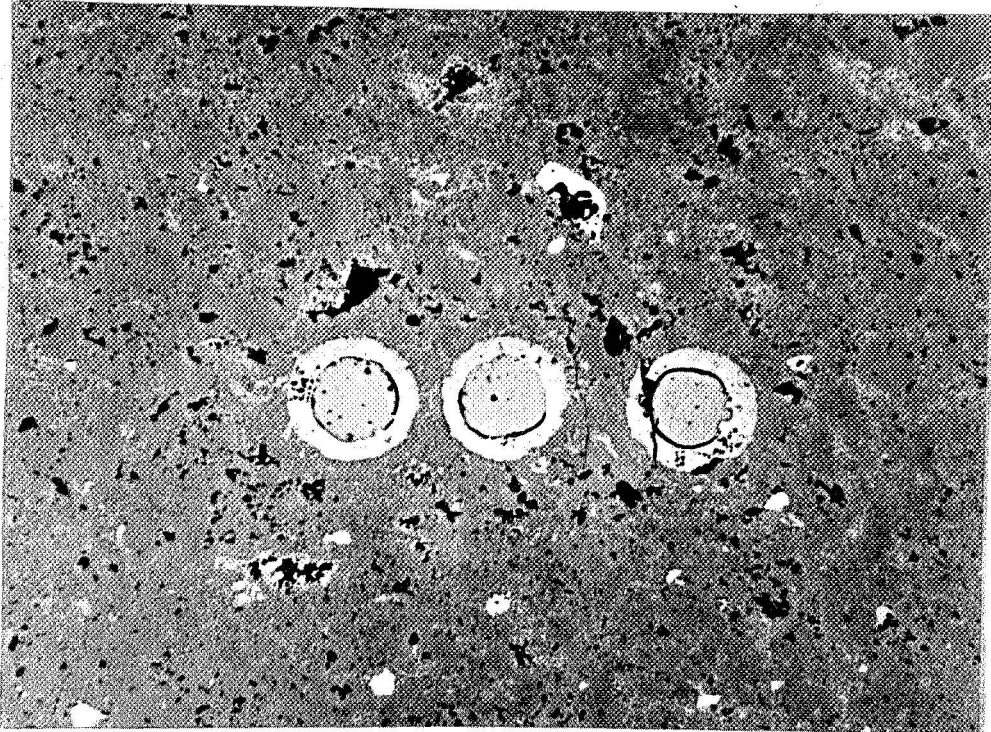
#5201-2                                                    500X

Figure 21.   Polished Section of $Si_3N_4$ Showing Carbon Mono-
filament.   Billet 1289
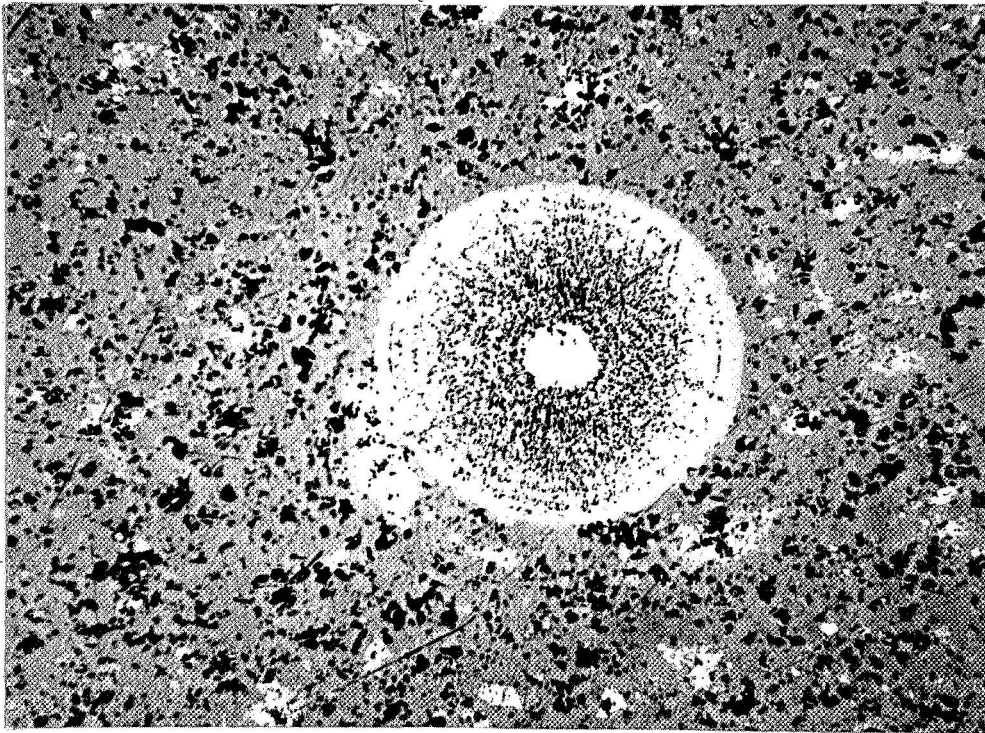


#5201-3                                                    500X

Figure 22.   Polished Section of $Si_3N_4$ Showing SiC Monofilament.
Billet 1289

the matrix having both its tungsten core and surface unreacted and in good condition. On the polished section, just a hole remained where the Tyco sapphire filament had been. This is not to say that the filament disappeared but that it became severely cracked all along its length and in depth, and thus could not be polished. It, then, cannot be used as a strengthening material for $Si_3N_4$ due to the break-up, resulting presumably from the large thermal expansion difference between $Si_3N_4$ and $Al_2O_3$. ( $\beta$-$Si_3N_4$ is 1.53 x $10^{-6}$°$F^{-1}$, (2.75 x $10^{-6}$°$K^{-1}$), $\alpha$-$Al_2O_3$ is 4.45 x $10^{-6}$°$F$ (8.2 x $10^{-6}$°$K^{-1}$)). Figure 23 shows the form SiC whiskers take when present in areas of 100 v/o loading in the SiC matrix. Some texturing is evident together with some cracking. However, when etched and under higher magnification, Figure 23b, the whisker morphology is clearly seen. Thus, whiskers may be retained as such in $Si_3N_4$ when hot pressed at 3272°F (2073°K). Finally, the Thornel yarn was seen with traces of reaction zone surrounding it.

To summarize, $Si_3N_4$ can be pressed to high density to what was shown to be a fine grain size with a $\beta$-$Si_3N_4$ structure. Composites having filamentary additions are possible at least in the case of SiC mono-filament and for SiC whiskers which retain their morphology. Further, graphite filaments can be used as monofilaments and may be used as yarn provided that in the latter case, provision is made to allow the nitrogen formed during the formation of a SiC reaction zone to escape and so prevent bloating. A billet (1336) was, therefore, prepared using SiC monofilament for testing in the thermal stability/thermal shock phase. The SiC monofilament was wound on a drum prior to making mats for a composite pressing in $Si_3N_4$. Extreme difficulty has been encountered in this area due to the very weak nature of the filament which continually breaks during winding and is very difficult to handle. However, billet 1336 was fabricated with SiC mono-filaments arranged in 15 equally spaced mats was fabricated and the NDT examination showed the mats to be unbroken and all lined up unidirectionally and bonded to the $Si_3N_4$.

The use of carbon monofilament as a fibrous additive was abandoned due to the extreme brittleness of the filament and the difficulty experienced in handling it.

In a previous section it was shown that very high temperature pressing conditions required to hot press SiC seemed to preclude any material other than carbon. However, because $Si_3N_4$ can be consolidated at 3272°F (2073°K) there may be a possibility of incorporating a metallic wire or fiber in $Si_3N_4$. A list of metals having melting points in excess of 3272°F (2073°K) was compiled and the free energy of formation of their nitrides versus temperature obtained.[9] These were arranged graphically and have been presented with the data for $Si_3N_4$[10] in Figure 19. The values for SiC were also included so that the following reaction is included:

$$1/2 \ Si_3N_4 + 3/2 \ C \quad \longrightarrow \quad 3/2 \ SiC + N_2 \quad\quad (2)$$

Thus, the only metals which are compatible thermodynamically are molybdenum and chromium. Rather surprisingly, the data indicate that tungsten will form a nitride above 2480°F (1633°K) at 1 atmosphere (1.01 x $10^5$ N/m$^2$).
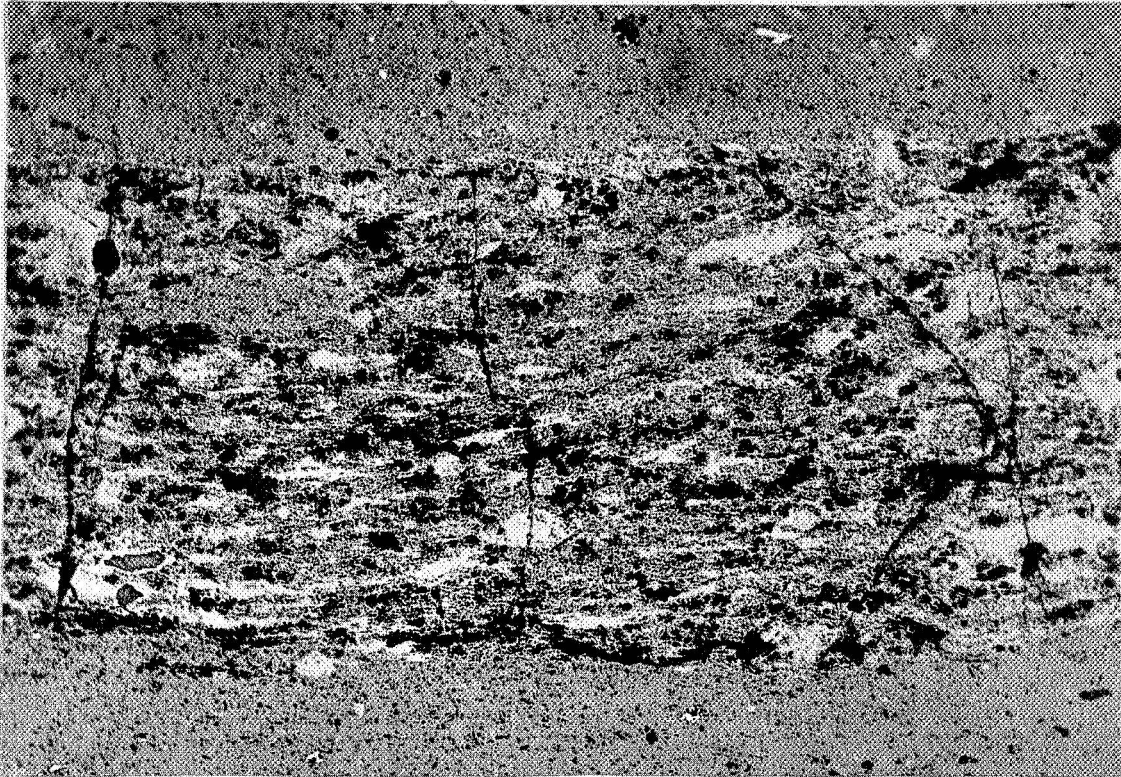
#5201-5                                                    100X

Figure 23a.   Polished Section of $Si_3N_4$ Showing SiC Whisker
              Zone.  Billet 1289



#5201-6                                                    500X

Figure 23b.   Etched Section of $Si_3N_4$ Showing SiC Whisker
              Zone.  Billet 1289

Chromium was rejected as a candidate because of its un-availability as wire and its relatively low melting point, $3406°F$ ($2146°K$). Some molybdenum wire and tungsten were chosen because of their high temperature properties and since the high pressure conditions will modify the thermodynamics and suppress the formation of $W_2N$, and also the kinetics of the reaction between nitrogen and tungsten have been reported to be very slow.[11] Rhenium was also chosen since although no thermodynamic data for its nitrides could be found, it was reported[12] that the nitride has a low stability and cannot be formed from nitrogen and rhenium. No judgement concerning the selection of materials based on the possible formation of silicides could be made because of the paucity of thermodynamic data relating to silicides.

A trial billet was pressed (1377) containing tungsten, molybdenum and rhenium wires and some coarse SiC whiskers obtained from Norton Co., but reaction between $Si_3N_4$ and the die body resulted. The degree of compatibility of the additives with $Si_3N_4$ was, therefore, inconclusive.

A billet containing only molybdenum wires was, therefore, fabricated. Thirteen layers of 3 mil ($7.92 \times 10^{-5}$ m) diameter molybdenum wires arrayed in mats with 1 mil ($2.54 \times 10^{-5}$ m) between each wire were pressed with $Si_3N_4$ in billet 1397. Although the molybdenum remained with no visual diffusion of molybdenum into the matrix, the molybdenum became very brittle. Analysis by the Debye-Scherrer x-ray diffraction technique showed that the remnants of the wires consisted principally of an impurity stabilized $Mo_5Si_3$ phase. No metallic Mo, Mo oxides or nitrides, $Si_3N_4$, $SiO_2$ or SiC were detected. Unprotected molybdenum cannot, therefore, be used as a ductile phase in $Si_3N_4$.

IV. COMPOSITE EVALUATION

A. Test Philosophy

A program was devised which would determine the feasibility of improving the mechanical behavior of high temperature composites to such a degree that they become materials for use as turbine stator vanes in advanced turbine engines. The high temperature compound systems which were studied were SiC and $Si_3N_4$ alone and with filamentary additions such as SiC whiskers, graphite monofilament, graphite yarn and SiC monofilaments to make composites.

The program was devised to improve the mechanical shock resistance (which was of primary importance), the thermal shock resistance and the stress-rupture life of these high temperature composites. All the composites were fabricated by hot pressing and were tested according to the following sequence of screening tests:

1. Thermal Shock Resistance

Thermal shock tests which included 100 thermal cycles from room temperature to 2400°F (1589°K). Each cycle consisted of inserting a sample at room temperature into a high temperature air stream which heated the sample to an equilibrium temperature of 2400°F (1589°K) (in not more than two minutes) followed by rapid cooling of the sample to room temperature (in two to three minutes).

2. Stability

Stability tests involved heating of specimens for 100 hours at 2400°F (1589°K), in an air environment with one two-to-three minute cycle each hour. The tested specimens were then examined for changes in weight, dimensions, compositions, microstructure, etc. The thermal shock and stability tests were combined into a single test.

3. Mechanical Shock Resistance

Standard impact tests were run on specimens of promising materials at room temperature, 2000°F (1366°K) to 2400°F (1589°K) with loads to produce up to five foot-pounds of impact (6.779J).

4. Stress Rupture Tests

Promising materials were stress-rupture tested in air at various temperature and stress levels to determine the stress-dependence of rupture life in the range of 2000°F (1366°K) to 2400°F (1589°K). The test comprised of testing in the bending mode using a four-point dead load system.

B. Testing Sequence

Since thermal shock resistance and stability were considered to be of importance in this program, these two series of tests were run before other tests to avoid extensive testing of materials which offer little potential for the desired application.

Where possible, materials developed in the program were compared with ceramic materials commercially available. Where appropriate, the commercially available materials were tested alongside the ceramic composites arising out of the developmental program. The mechanical properties of the nickel-base superalloy B1900 and the cobalt-base superalloy X-40 were also measured within the confines of the program to compare the composites with currently available superalloys.

## C. Thermal Shock/Thermal Stability

The thermal shock and thermal stability tests were combined into one test. Several different SiC based materials were tested in order to assess the affects of variations in the base microstructure and also the effects of additions of carbon filaments and cloth and SiC whiskers. Plain $Si_3N_4$ was tested as well as material with additions of SiC in whisker and filamentary form. For comparison, two specimens of KT-grade SiC* were tested as well as a $ZrB_2$ based material and $Al_2O_3$.

The specimens were heated in a natural gas flame for a 1-hour cycle which involved a rapid cool to ambient and reheat once each hour. The tests were run for 100 hours with a specimen temperature of $2400^{\circ}F$ ($1589^{\circ}K$). The specimens were directly in the burner flame so that they were not uniformly heated, but would be cooler at the ends and would also have a thermal gradient from front to back. This condition was desired in order to simulate more closely the environment of a gas turbine. The specimen was cooled by rapid retraction from the furnace into an air blast to ambient temperature in approximately $2\frac{1}{2}$ minutes. The specimens were $2\frac{1}{2}$" ($6.6 \times 10^{-2}$ m) long x 1" ($2.54 \times 10^{-2}$ m) wide and taper from $\frac{1}{2}$" ($1.27 \times 10^{-2}$ m) to 1/8" ($3.3 \times 10^{-1}$ m) in thickness. The heating and cooling blasts were directed at the thin edge.

The actual test apparatus is shown in Figure 24. The bars were placed horizontally and held without constraint at the ends in an Inconel frame which formed a part of the burner chimney; the frame holds five specimens lined parallel. The specimens were directly over a series of burners on a common manifold so that each specimen was directly over a burner. In order to cool them, the Inconel frame was retracted by an air cylinder so that the specimens were aligned above a row of nozzles which provided a cold air blast. The air cylinder was automatically controlled so that it retracts for 2.5 minutes once each hour and then returns to the burners. The system was constructed and tested to provide a temperature of $2400^{\circ}F$ in the hottest part of the flame where the specimen was located. The calibration of the system is presented in Appendix B.

The results are presented in Tables 6a and b. For reasons of convenience, the unit was occasionally run for other than 1-hour cycles so both total shocks and total exposure is reported; only the actual time at temperature, not the total cycle time is reported for the exposure time. In addition, several specimens received a considerable number of thermal shocks at somewhat lower temperatures during the set-up period; these are also shown in the table.

---

* Obtained from Carborundum Co.
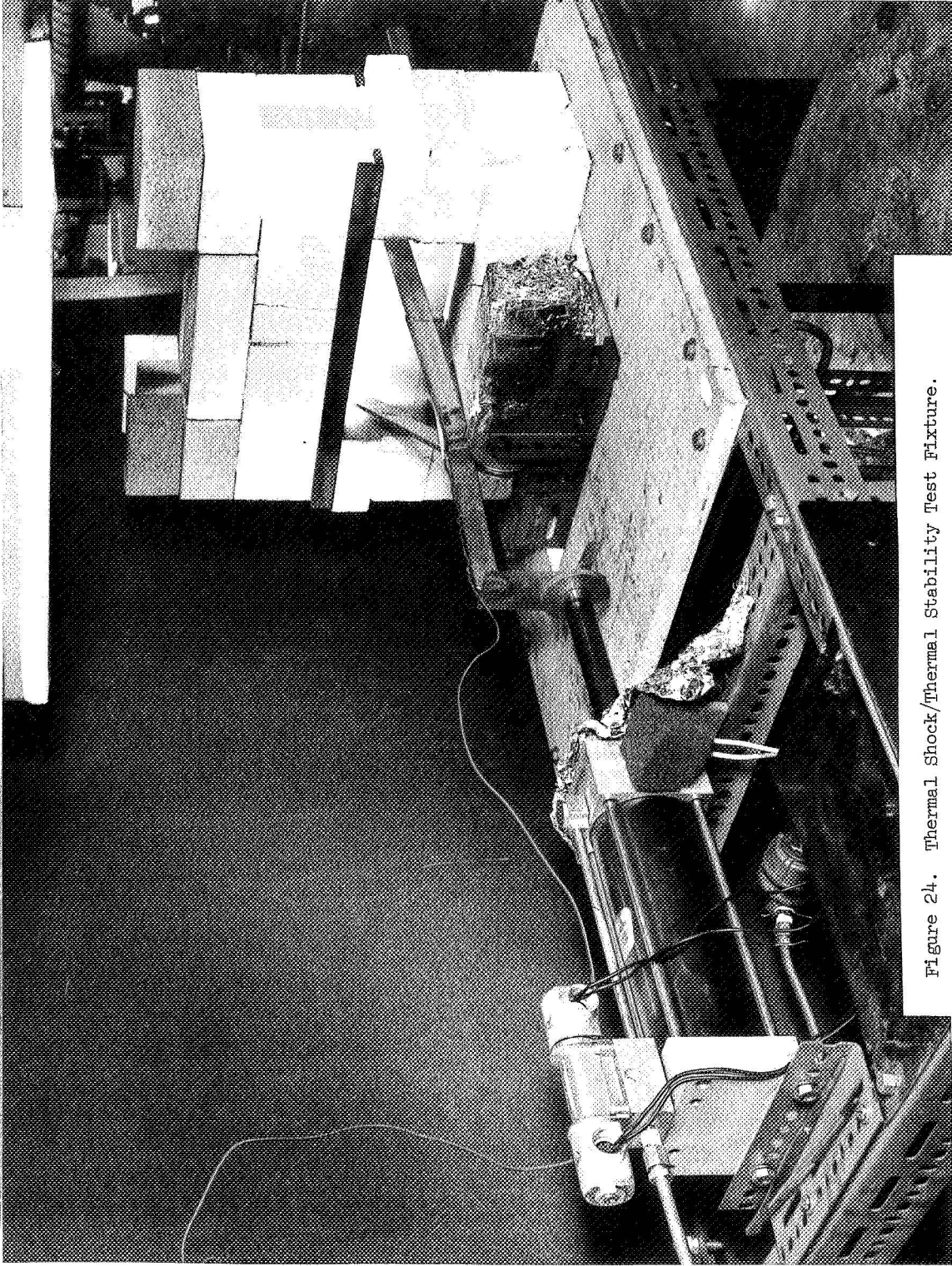
Figure 24. Thermal Shock/Thermal Stability Test Fixture.

TABLE 6a

THERMAL SHOCK/THERMAL STABILITY RESULTS FOR SiC

| Material | 1230 SiC | 1233 SiC | 1237A SiC | 1237B SiC | 1275 SiC | 1293 SiC | 1250A SiC + Thornel | 1250B SiC + Thornel | 1316 SiC + SiC (w) | 1393 SiC + C (cloth) | KT-1 | KT-2 |
|---|---|---|---|---|---|---|---|---|---|---|---|---|
| Additives | 3A | 3A 3C | 3A 1C | 3A 1C | 1A 3C | 3A 1C | 3A 1C | 3A 1C | 3A 3C | 3A 3C | | |
| Total Shocks T≈2350°F (1561°K) | 15 | 100 | 315 (316)+ | 73 (99) | 102 | 14 | 36 | 30 | 120 | (30) | 197 | (30) |
| Total Shocks T≈2000°F (1366°K) | 15 | 134 | 350 (351) | 104 (130) | 102 | 20 | 42 | 36 | 120 | (30) | 197 | (30) |
| Total Exposure 2400°F (1589°K) hrs. | 13 | 150 | 338 (340) | 127 (147) | 86 | 21 | 36 | 34 | 102 | (28) | 163 | (28) |
| Number of Shocks After Cracks Obs. | 25 | N.C.* | 2 | 26 | 2 | 3 | 47 | 13 | N.C. | (52) | N.C. | Removed |
| Exposure Time After Cracks Observed. Hrs. | 21 (broke in 4 pieces) | | 1 | 22 | 2 | 2 | 39 | 7 (broke in 2 pieces) | N.C. | (41) (badly de-laminated) | 1 | |
| Weight Before (g) | | | 39.170¹ 39.166 | | 40.582 | 39.174 | 34.658 | 35.495 | 38.850 | | 39.614 39.631 | 41.097 |
| Weight After (g) | | | 39.150 | | 40.590 | 39.186 | 35.345 | 35.905 | 38.844 | | 39.618 + 0.043% | 41.110 |
| Change | | | -0.051% | | +0.020% | +0.031% | +1.99% | +1.15% | -0.016% | | + 0.010% | +0.032% |

*N.C. - No cracks observed by the end of the test.

+The values in parentheses are for the last round of tests which were after the unit was modified making the thermal shock more severe.

¹This only covers the last 214 hours.

## TABLE 6b

### THERMAL SHOCK/THERMAL STABILITY RESULTS

| Specimen Material | $Si_3N_4$ 1251A | $Si_3N_4$ 1251B | $Si_3N_4$ 1262 | $Si_3N_4$ 1336 | $Al_2O_3$ C59A | $Al_2O_3$ C598 |
|---|---|---|---|---|---|---|
| Additives | 5M 2C | 5M 2C | 5M 2C | 5M 2C | 0 | 0 |
| Total Shocks T 2350°F (1561°K) | 117 | 73 (153)/ | 210 (289)/ | 30 | 1 | 1 |
| Total Shocks T 2000°F (1336°K) | 148 | 102 (182)/ | 216 (295)/ | 30 | | |
| Total Exposure 2400°F (1589°K) | 167 | 127 196 | 188 254 | 23 | 1 | 1 |
| Shocks After Cracks Observed | NC | NC | NC | 2 | Removed | 1 |
| Exposure After Cracks Observed | | | | 1 | | 1 |
| Weight Before (g) | 40.931* | | 40.206 40.347 | 41.003 | 50.572 | |
| Weight After (g) | 40.919 | | 40.347 40.306 | 41.097 | 50.571 | |
| Change | | -0.029% | +0.25% | +0.22% | | |

* This only covers the last 40 hours.

/ The values in parentheses are for the last round of tests were made after the unit was modified making the thermal shock more severe.

The bars were frequently observed during the cooling cycles for evidence of cracking. Cracks are best seen while the specimen is cooling as a result of the temperature differences across them. The specimens were usually allowed to continue for several cycles after the first observation of cracks. Several specimens were allowed to continue for many cycles to determine whether they would break into several pieces. If cracks had not been observed sooner, testing was usually discontinued a short time after the target test durations of 100 hours of exposure and 100 thermal shocks from $2400^\circ F$ ($1589^\circ K$) were reached; a few were allowed to go longer to assess eventual lifetime.

For the last round of testing, the inside of the Inconel box was insulated to increase its lifetime. The ends of the specimens extended into the insulation which apparently had the effect of making the thermal shock more severe. The results of this round of testing are all enclosed in parentheses in the table.

### 1. Silicon Carbide

The results show some differences in the thermal shock resistance of the various SiC based materials. The materials with high density, fine grain size and little or no second phase were the best. It is seen that the plain materials 1233 and 1237 and similar material with a SiC whisker addition, 1316, survived the test for over 300 cycles before modification of the box increased the severity of the test. After the modifications all of the SiC based materials cracked in a relatively short time indicating the test had been made more severe.

Although the one sample of KT-type SiC showed no observable cracks during testing, examination afterwards revealed fine cracks in it; similar cracks were not seen in the hot pressed bodies which had no large cracks. This difference probably results from the fact that the KT type material is not as strong as the hot pressed material so that less elastic energy is stored in the body at the point of crack initiation and it can be relieved by the small cracks which do not subsequently propagate.

Failure usually occurred by a vertical crack in the center of the specimen directly above the gas nozzle. In a few cases, several cracks developed. The most probable causes of failure of those specimens which failed early are as follows.

Specimen 1230, which failed early, was only 90% dense, which would lower its strength and thermal conductivity. Specimen 1275 which failed near the end of the test had a rather large grain size (18 $\mu$m) which would lower its strength. Specimen 1293 had a large grain size (45 $\mu$m) and considerable second phase; the second phase is thought to be $Al_2O_3$ which has a higher thermal expansion than SiC. Comparison of 1293 and 1275 suggests the second phase is probably more aggravating than the large grain size.

The SiC specimens exhibited excellent dimensional stability with only limited surface oxidation and erosion. A photograph is shown in Figure 25
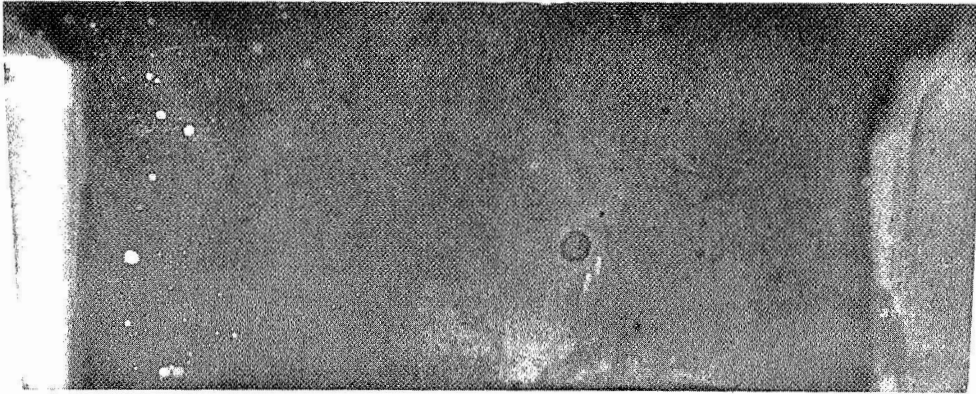
#5309-6                                                    2X

Figure 25.   SiC Billet 1233 After Thermal Cycle Tests.
             150 hours exposure at 2400°F (1589°K).

of specimen 1233 after 150 hours of exposure. The weight change data
indicate a small initial weight gain as the oxide coating develops. After
longer times the weight slowly decreased indicating the oxidation rate was
balanced by loss of material presumably by evaporation and/or erosion. For
the hot pressed materials the peak in the weight gain appears to occur in
the vicinity of 50 hours; for the KT material it was at a somewhat longer time.

The specimens with Thornel yarn exhibited rather low shock
resistance. The matrix density of these was quite low (comparable with 1230)
and this may be the cause; comparison with billet 1230 $(SiC + 3$ w/o $Al_2O_3)$
in fact, indicates a better lifetime for the Thornel additions. Examination
of the specimen indicated that the crack was diverted each time it encountered
a row of Thornel. The two specimens tested had normal SiC surface oxidation,
but abnormally high weight gain. Microstructural examination indicated
oxidation of the internal surfaces of pores in the SiC was the cause of the
weight gain. This examination also indicated most of the carbon was lost
by oxidation. If the specimens had been sufficiently dense to be impermeable
to oxygen, it seems likely the rate of loss of the carbon would have been
slower.

Specimen 1393 made up of SiC with graphite cloth, delaminated during
the test; this was presumably caused in part by oxidation of the graphite.
There was not enough $SiO_2$ of appropriate viscosity to flow and coat the
graphite to afford protection.

## 2. Silicon Nitride

The $Si_3N_4$ specimens had excellent resistance to thermal shock.
These bodies survived even after the severity of the test was increased.
The improved performance relative to the SiC is thought to be largely a result
of the lower thermal expansion of $Si_3N_4$; it is interesting, however, that
1262 which had a 25 v/o SiC whiskers in $Si_3N_4$ indicated no problem from the
difference in expansion of the two phases. The only $Si_3N_4$ based material
to fail was 1336 which had SiC monofilaments in it; this cracked along the
plane of the filaments.

The $Si_3N_4$ specimens exhibited much greater build up of surface
oxide as seen in Figure 26 and much more rapid weight gain than the SiC, as
with the SiC, the weight gain is rapid initially, and then levels off and
eventually drops as a result of erosion and evaporative losses. The peak
in the weight gain is in the range of 125 hours. The front tip of the
$Si_3N_4$ was slightly rounded by erosion and oxidation in contrast to the SiC
which remained remarkably square as can be seen in Figure 27.

As seen in Figure 26, the oxide shows evidence of being molten at
temperature and frequently has a frothy appearance as though a gas is being
lost from within it; in some specimens the oxide was washed away from the
front edge by the gas flow. In static oxide tests, this oxide has been
shown to contain $MgSiO_3$.*

In summary, the $Si_3N_4$ bodies exhibited excellent resistance to
thermal shock; the testing was not severe enough to determine the effect of

---

* W.A. Sanders, NASA Lewis, private communications.
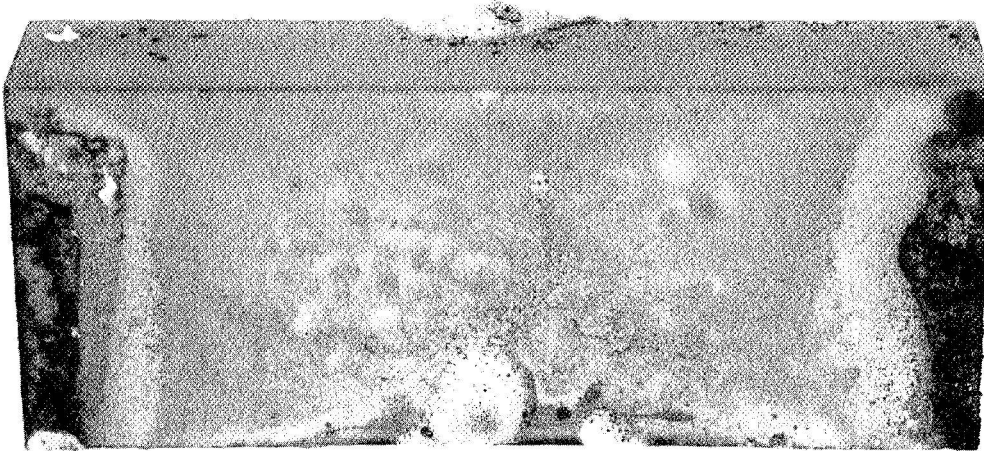
#5309-7                                                    2X

Figure 26.   Si$_3$N$_4$ Billet 1251A After Thermal Cycle Tests.
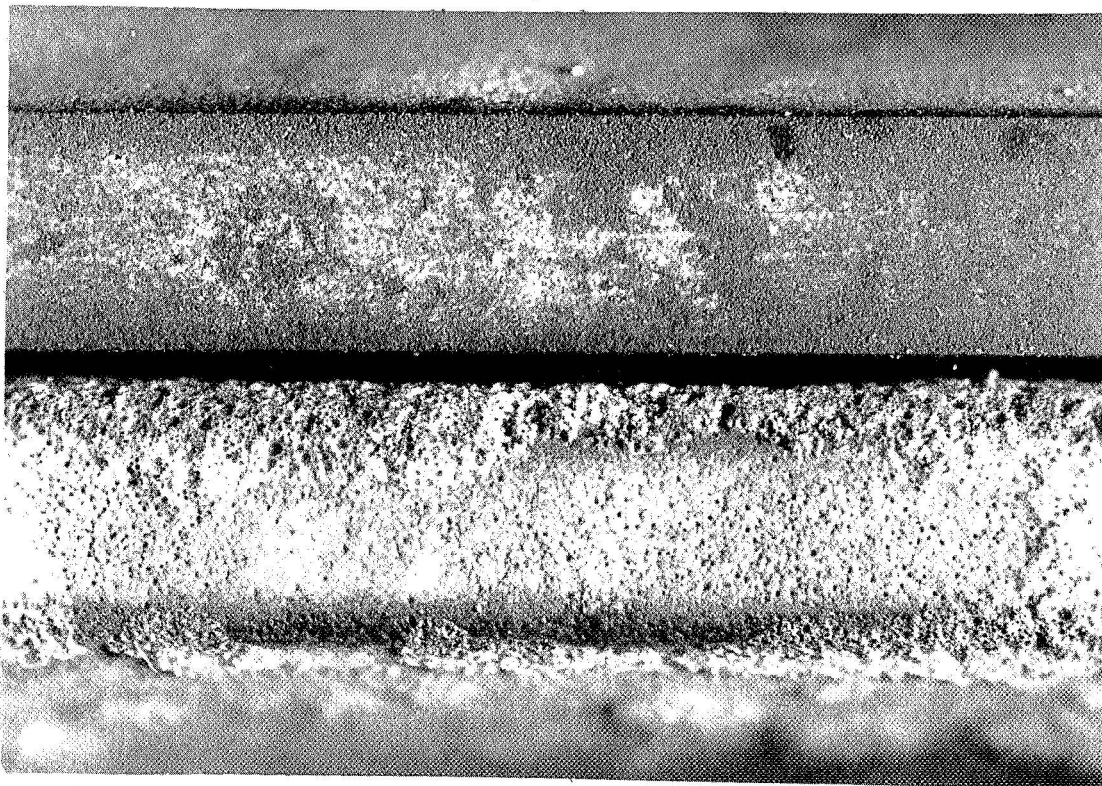


#5309-4                                                    10X

Figure 27.   Comparison of Front Edges of SiC Billet 1233 Top
             and Si$_3$N$_4$ Billet 1251 Bottom Showing Greater Loss
             of Material by Erosion and Oxidation in the Si$_3$N$_4$.

whisker additions to the $Si_3N_4$ on thermal shock resistance. The finer grained dense SiC materials with a minimum of second phase exhibited good shock resistance although they were inferior to the $Si_3N_4$ materials. Both SiC and $Si_3N_4$ materials have good oxidation resistance with only minimal material loss; however, the $Si_3N_4$ materials are inferior to SiC in retaining dimensional stability because of greater erosion and oxidation rates. Although $SiO_2$ is probably present on the SiC surface, $MgSiO_3$ is found on the oxidized surface of $Si_3N_4$ presumably derived in part from the MgO densification additive. If the amount of MgO can be reduced during hot pressing or can be removed subsequently, the oxidation of $Si_3N_4$ would result in $SiO_2$. A lower oxidation rate may ensue and this should be an incentive in obtaining a lower MgO containing body.

### 3. Other Material

For comparison (Table 6b) two specimens of $Al_2O_3$ were tested. Not surprisingly, the $Al_2O_3$ specimens cracked badly on the first shock.

### D. Mechanical Shock Resistance

An impact tester of the Bell Telephone Laboratories type was modified to provide impact strength data at temperatures from room to 2400°F (1589°K). There is no standard test described for ceramic materials at elevated temperatures by the ASTM. However, the modified instrument does conform to the requirements of specification D256 - standard method of test for impact resistance of plastics and electrical insulating materials. In order to provide comparison data, specimens of two superalloys were also tested. A nickel base - B1900, and a cobalt base material - X40, were chosen for this purpose. In order to accomplish this comparison, the impact tester was been modified to include some of the requirements of ASTM E23-66-Standard methods for notched bar impact testing of metallic materials. In this respect, specimens 0.250 inch ($6.6 \times 10^{-1}$ m) x 0.250 inch ($6.6 \times 10^{-1}$ m) in cross section, 2.165 inches ($5.72 \times 10^{-2}$ m) long with a 1.574 inch ($4.15 \times 10^{-2}$ m) gage length in a Charpy test mode were used. All the ceramic composite materials were tested using a 2-foot pound (2.71J) hammer while a 16-foot pound (21.7J) hammer was used for the superalloys. It was decided not to notch any of the metal or ceramic specimens and this constitutes a departure from both ASTM D256 and ASTM E23-66.

Although the possibility of jamming after breaking is greater in the Charpy (simple beam) mode of impact testing, this method was chosen. In the Izod (cantilever beam) mode, there is an even greater problem in maintaining a properly clamped specimen particularly when high temperatures in air are to be used.

The Bell Telephone Laboratory impact tester was modified in the following fashion to provide impact strength data up to 2400°F (1589°K) in air. The bearing for the Charpy hammer was removed and placed in a sturdy angle iron frame which itself could be adjusted to be level by means of threaded legs. The bearing was mounted in such a way that the scale, release mechanism, anvils for the specimen and pendulum could be used as in the original machine with no change in relative dimensions. The specimen, however,

was mounted within a furnace which comprised of two halves. Each half of the furnace contained three SiC heater rods mounted appropriately in fire-brick. The furnace was closed by a removable fire-brick lid and two end plugs. When the temperature of the furnace reached the required value as measured by a thermocouple, the lid and end plugs were removed, the Charpy hammer released and the impact energy recorded on the dial. The time between the removal of the lids and impact is only a few seconds and no significant cooling or the sample took place. Because of the unavailability of rigid, oxidation resistant alloys for use at 2400°F (1589°K), the anvils for the test specimen have been made from ceramic. SiC was chosen as anvil material to reduce any contamination or corrosion between the anvil and the silica formed on SiC or $Si_3N_4$ specimens during heat up. These were mounted on a fire-brick, properly grooved to permit free passage of the Charpy hammer. The whole assembly could be adjusted in a horizontal sense to accommodate any maladjustment between the vertical line of the pendulum bearing and the specimen surface which may occur at temperature due to the thermal expansion of components.

A photo of the modified impact strength measuring device is shown in Figure 28 with the furnace top removed in the position ready for a strength determination to be made using the 2 ft.-lb. (2.71J) hammer. The machine was calibrated for windage and friction. The hammer mass was measured and the total height through which it fell determined. The center of percussion was checked to be in the center of the hammer anvil by determining the length of the simple pendulum equivalent to the hammer. Finally, the specimen was adjusted to be square in the anvils and the hammer vertical at the point of impact. The temperature of the specimen was determined using a platinum/platinum-rhodium thermocouple placed close to it, but not to impede the impact measurement. At temperature, the components expand and the adjustments may need correcting. Thus, a gage length of stainless steel was made to check anvil distance. That the hammer was vertical at the point of impact could not be determined since the hammer could not survive long enough in the hot furnace. However, from witness marks on the hammer anvil, it was clear that the specimen had remained square and at the center of percussion. Finally, at the end of the series of measurements, the windage and friction losses were measured and found to be unchanged.

### 1. Silicon Carbide

The results of the impact tests are presented for SiC in Table 7. They indicate that the impact strength of SiC does not change much at high temperature compared with the room temperature values. The difference between 2000°F (1366°K) and 2400°F (1589°K) is probably within the range of uncertainty of the errors involved and no conclusions should be drawn from this magnitude.

Of all the SiC billets tested, billet 1237 has the highest impact strength. Although a fine-grain material, 1237 is not the finest grain size material of the series (billet 1233 being the finest at 8.3 μm). The SiC material having a 6 w/o addition of $Al_2O_3$ (billet 1293) has an approximate grain size of 50 μm, but compares closely in impact strength to the fine-grained material. This indicated that at least in the case of SiC, the grain size does not effect the value of the impact strength but is thought to be important in terms of creep strength.
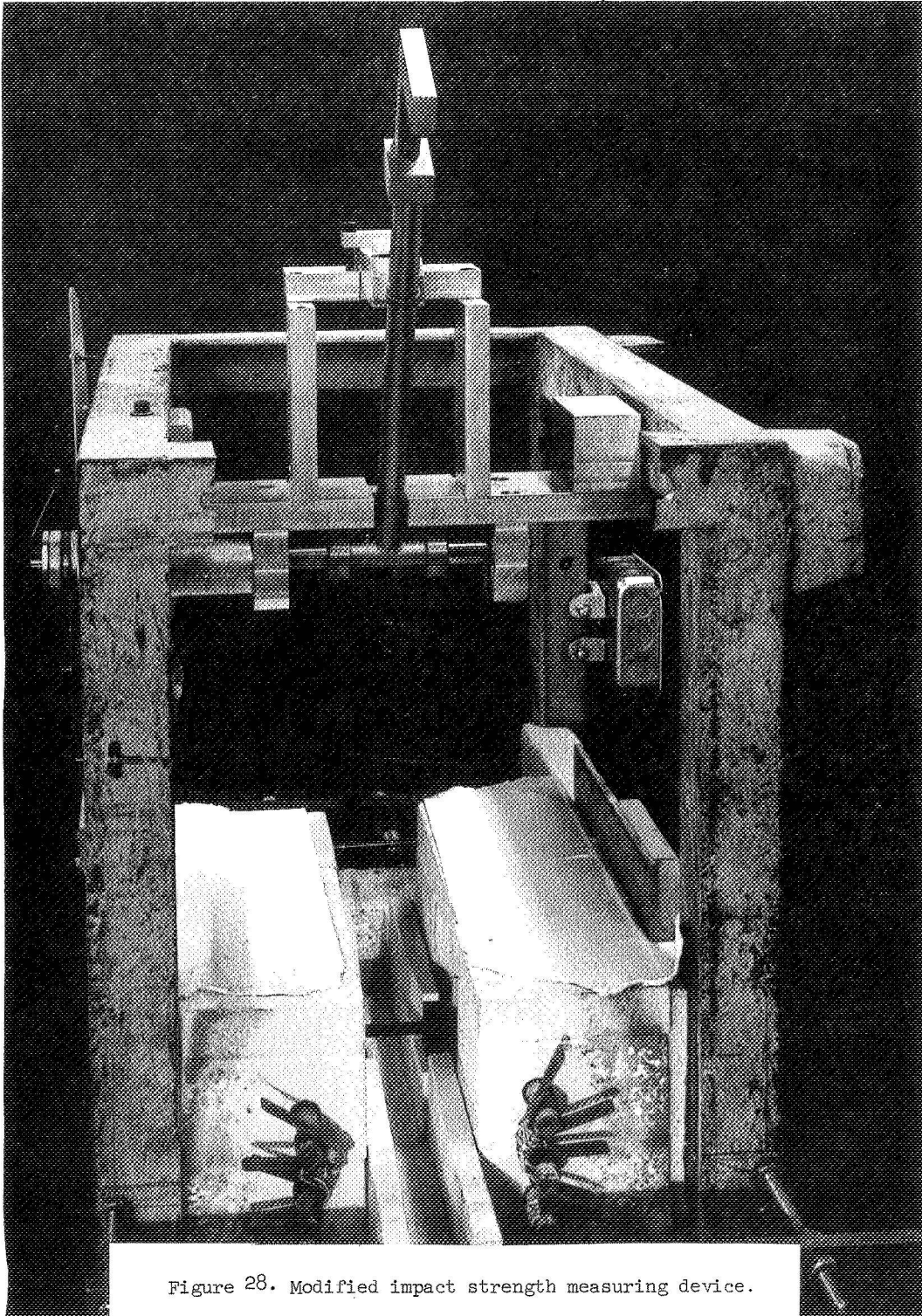
Figure 28. Modified impact strength measuring device.

## TABLE 7

### IMPACT TEST RESULTS FOR SILICON CARBIDE

| Billet | Material | Grain Size μm | Density gm/cc | Impact Strength in.-lbs. | | | Impact Strength J | | |
|---|---|---|---|---|---|---|---|---|---|
| | | | | Room Temp. | 2000°F | 2400°F | R.T. | 1366°K | 1589°K |
| 1230 | SiC + 3 w/o Al2O3 | - | 2.88 | 0.52 | 0.43 | 0.40 | 0.0586 | 0.0486 | 0.0452 |
| 1233 | SiC + 3 w/o Al2O3 + 3 w/o C | 8.3 | 3.14 | 0.55 | - | 0.64 | 0.0622 | - | 0.0723 |
| 1237 | SiC + 3 w/o Al2O3 + 1 w/o C | 8 | 3.08 | 0.76 | 0.60 | 0.79 | 0.0852 | 0.0678 | 0.0893 |
| 1250 | SiC + Thornel (3 w/o Al2O3 + 1 w/o C) | - | 2.86 | 0.59 | 0.67 | 0.48 | 0.0676 | 0.0746 | 0.0542 |
| 1275 | SiC + 1 w/o Al2O3 + 3 w/o C | 18 | 3.19 | 0.59 | 0.56 | 0.73 | 0.0676 | 0.0632 | 0.0825 |
| 1293 | SiC + 6 w/o Al2O3 + 3 w/o C | 45 | 3.25 | 0.62 | 0.60 | 0.48 | 0.0700 | 0.0678 | 0.0542 |
| 1316 | SiC + 3 w/o Al2O3 + 3 w/o C + 25% SiC whiskers | 30 large 3.3 small | 3.09 | 1.6 | 1.44 | 1.35 | 0.180 | 0.163 | 0.153 |
| 1393 | Graphite Cloth in SiC Matrix Impact to Cloth | - | - | 1.15 | 1.2 | 0.865 | 0.130 | 0.135 | 0.0978 |
| 1409 | SiC Whiskers | 1 | 3.14 | 1.15 | 1.16 | 1.21 & 0.98 | 0.130 | 0.131 | 0.137 & 0.111 |

## TABLE 8

### IMPACT TEST RESULTS FOR SILICON NITRIDE

| Billet | Material | Grain Size μm | Density gm/cc | Impact Strength in.-lbs. | | | | Impact Strength J | | |
|--------|----------|---------------|---------------|---------------------------|------|------|--------|-------------------|----------|----------|
| | | | | Room Temp. | 2000°F | 2400°F | R.T. | 1360°K | 1589°K | |
| 1251 | Si₃N₄ + 5 w/o MgO + 2 w/o C | 2.5 | 3.19 | 1.05 | 1.50* | 1.31 | 0.1185 | 0.170* | 0.148 | |
| 1262 | Si₃N₄ + SiC Whiskers | 1 | 3.07 | 1.33 | 1.5 | 1.68 | 0.150 | 0.17 | 0.190 | |
| 1336 | Si₃N₄ + 5 w/o MgO + 2 w/o C + SiC filaments | - | 3.18 | 0.79 | 0.73 | 1.2 | 0.0893 | 0.0825 | 0.135 | |

_____

* Performed at 2200°F (1477°K)

## 2. Silicon Nitride

Silicon nitride has a higher impact strength than SiC (Table 8). The strength of $Si_3N_4$ also increases when heated to 2000°F (1366°K) and 2400°F (1589°K). The difference in absolute magnitude of impact strength between 2000°F (1366°K) and 2400°F (1589°K) for $Si_3N_4$ may not be significant although they vary by 10%.

## 3. Addition of Whiskers to Silicon Carbide

The impact strength was measured for billet 1409, pressed from essentially 100% whiskers and having an approximate grain size of 1 μm. Although the strength was higher than for SiC with no additives, it is nevertheless weaker than when only 25% whiskers are added to a SiC body (billet 1316). This suggests an optimum fraction of whisker additive to produce the highest impact strength.

Some fractographs of SiC composites tested in the impact tester were made. The fractures in the case of SiC (billet 1233) occur mostly in a transgranular fashion both at room temperature and at 2400°F with some increase in intergranular fracture at the higher temperature as shown in Figure 29. When whiskers are added (billet 1316) similar conditions prevail in terms of the fracture propagation. Some very angular and regular grains can be seen which may be the whiskers in the structure, as shown in Figure 30, which were retained in this billet pressed at a lower than normal temperature (c.f., Table 1).

The addition of SiC whiskers improve the impact strength of SiC. The increase is most marked for a SiC matrix where a 25 v/o addition of whiskers increases the impact strength from 0.55 (0.0622 J) to 1.6 inch pounds (0.18 J); that is, by over 3 times (c.f., billet 1233 and 1316 values at room temperature in Table 7).

## 4. Addition of Whiskers to $Si_3N_4$

The addition of SiC whiskers also improves the impact strength of $Si_3N_4$. Although the improvement for $Si_3N_4$ matrices is less dramatic at room temperature, there is a marked increase at the high temperature due in part to the effect of the $Si_3N_4$ matrix itself which has a higher impact strength the higher the temperature. Thus, although the highest impact strength at 2400°F (1589°K) for $Si_3N_4$ + 25 v/o SiC whiskers, if specimens from billets 1251 and 1262 (Table 8) are compared, the whiskers only contribute about a 27% increase in strength.

In the case of $Si_3N_4$, fractures occur predominantly by inter-granular paths both at room temperature and at 2400°F (1589°K) shown typically in Figure 31 in contrast to the SiC matrix fractures.

When whiskers are added, the incidence of transgranular cracking increases in comparison with the case for whisker additions to SiC (Figure 30a and b). Again, regular grains often of hexagonal cross-section can be observed which are thought to be the SiC whiskers. One such hexagonal grain was pulled out during replication and electron diffraction of the

#70386                                                    7500X

Figure 29a.   Fractograph at R.T. for Billet 1233.
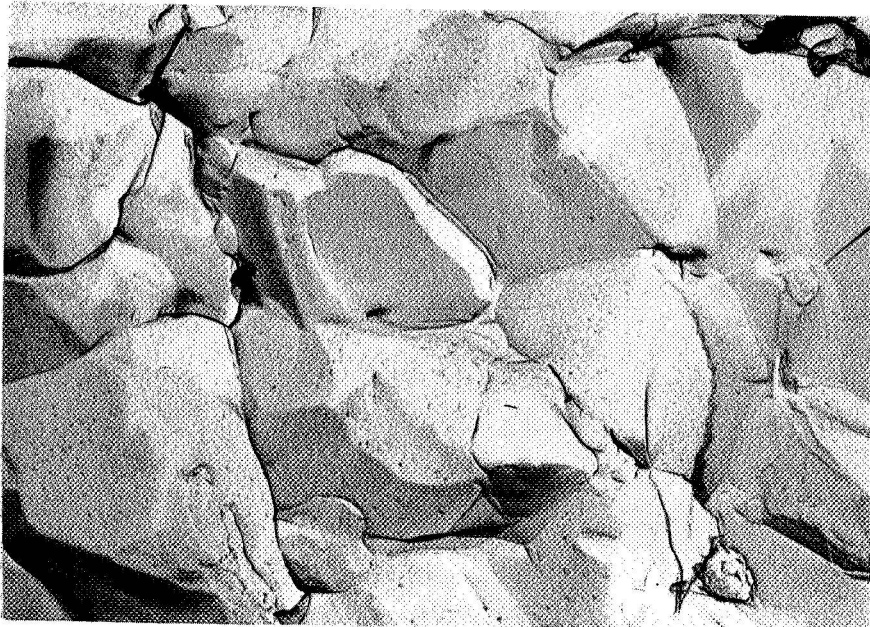


#70390                                                    7500X

Figure 29b.   Fractograph at 2400°F (1589°K) for Billet 1233.
              Density 3.14 gm/cc, Grain Size 3.3 μ.
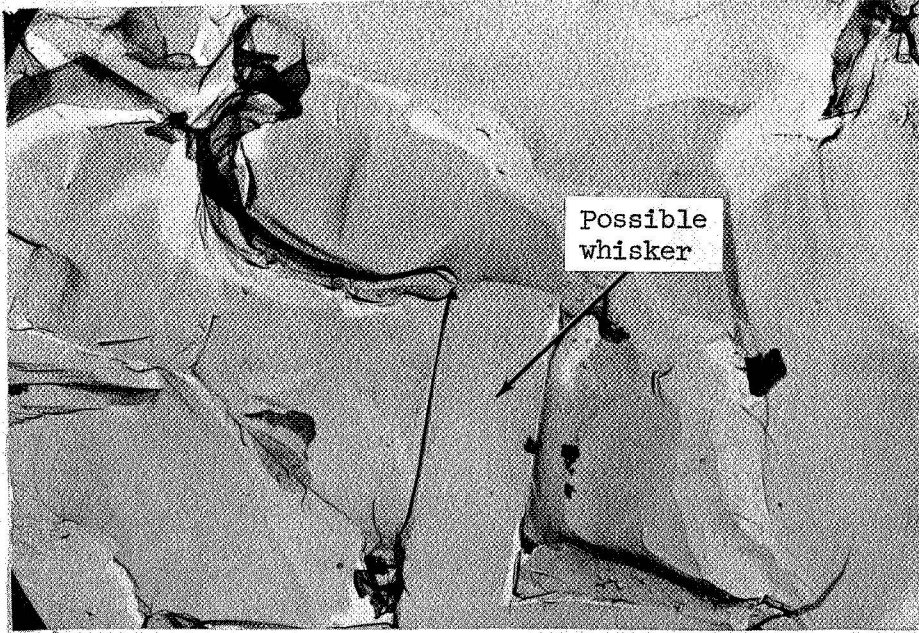
#70395                                                      7500X

Figure 30a.   Fractograph at Room Temperature for SiC.   Billet 1316
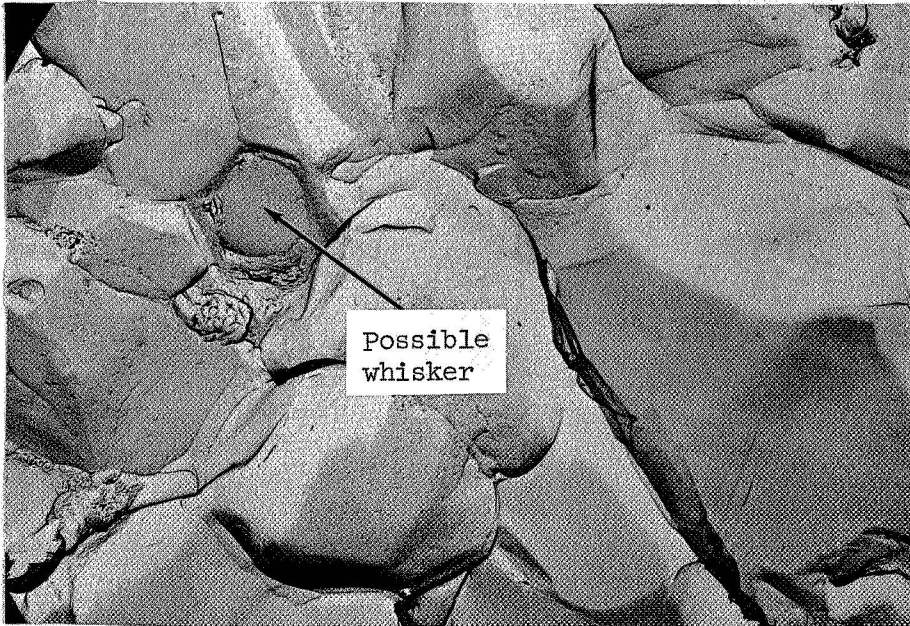


#70400                                                      7500X

Figure 30b.   Fractograph at 2400°F (1589°K) for Billet 1316.
              Density 3.09 gm/cc, Grain Size 3.3 μ Average,
              30 μ Largest Noted.

particle indicated that it indeed was SiC. Further, a riverlet pattern around the particle indicated that the crack front was interrupted when it encountered the whisker as shown in Figure 32.

The impact strength measured for specimens from bilet 1336 indicates that SiC monofilaments detract from the impact strength of the $Si_3N_4$ matrix when compared with the values for billet 1251 (Table 8).

### 5. Other Additives

Filamentary additives were thus shown to increase the impact strength of SiC and $Si_3N_4$ ceramic matrices. Although Thornel filament in small quantities did not improve the strength (billet 1250 in Table 7), graphite filaments arranged unidirectionally and bonded with graphite derived from an infiltrated phenolic after appropriate heat treatment, gave encouragingly high strengths both at room temperature and high temperature. For example, the Carbitex material in Table 9 retains over 8 in.-lbs. (0.966 J) impact strength at 2400°F (1589°K). Of course, the rapid oxidation of such materials causes their rejection for use in gas turbines. The specimens after fracture, show a stepped structure at the opposite end of each broken piece indicating the sliding of the layers over each other. A stress versus time curve obtained at approximately $10^{-5}$ $sec^{-1}$ strain rate is shown in Figure 33 and indicates how the graphite behaves, and why a high impact strength results. It seemed possible that the incorporation of enough graphite filaments may add significantly to the strength of SiC, while the SiC matrix conferred oxidation resistance to the carbon. This then was the philosophy which prompted the fabrication of such graphite filament/SiC composites. The graphite cloth in SiC (billet 1393) showed promising impact strength compared with SiC (Table 7). The strength was not, however, as high as for the whisker additions to SiC (billet 1316). Taken with the results for oxidation resistance, it is clear that SiC alone cannot confer enough resistance to oxidation to carbon. If improved oxidation resistance is achieved, then higher strength graphite should be used if substantial increases in impact strength are to be realized.

For the comparison of strengths with currently available material, KT SiC, B1900 and X-40 (HS 31) were tested for strength in impact. Because the solidus would be exceeded in the case of the alloys, these were only tested to 2300°F (1533°K). Further, the room temperature strengths of the alloys exceed the capacity of the Bell Laboratory's impact tester with the largest hammer available and so only high temperature values were measured.

The nickel-base alloy (B1900) demonstrated decreasing impact strength with increasing temperature. The cobalt base alloy exhibited increased ductility as the temperature increased and absorbed the full 16 ft. lbs. (21.7 J) of the hammer while bending to the included angle shown in Table 9. The KT SiC increased in impact strength at 2400°F (1589°K) presumably due to the increase in ductility by virtue of the silicon second phase present in the material.

### E. Stress Rupture Testing

Four materials were selected for stress-rupture evaluation at
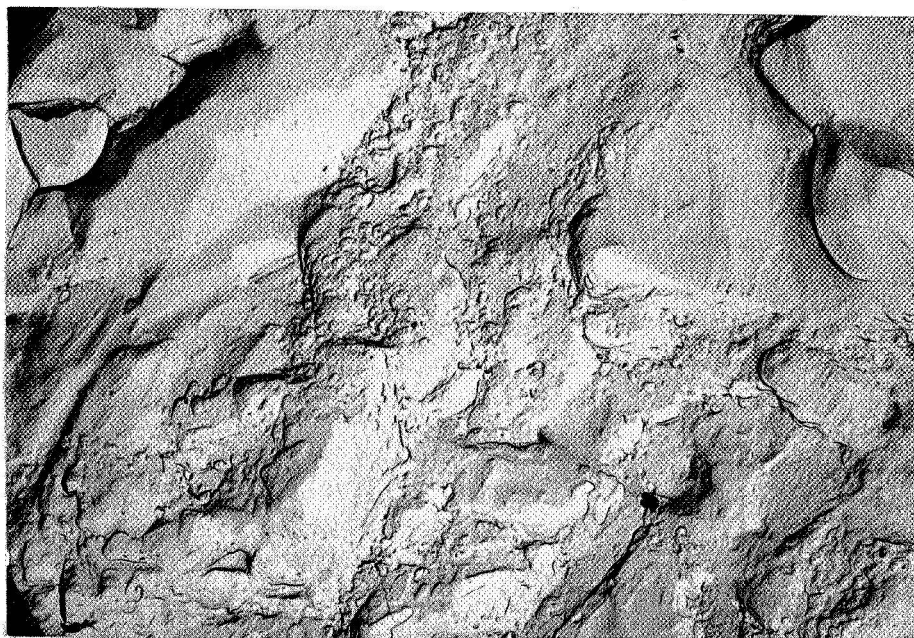
#70370                                        7500X

Figure 31.   Fractograph of Si3N4 Billet 1251 Broken at 2000°F
             (1366°K).  Density 3.19 gm/cc, Grain Size .2 μ -
             Small, 2.5 μ Large.



Possible
whisker
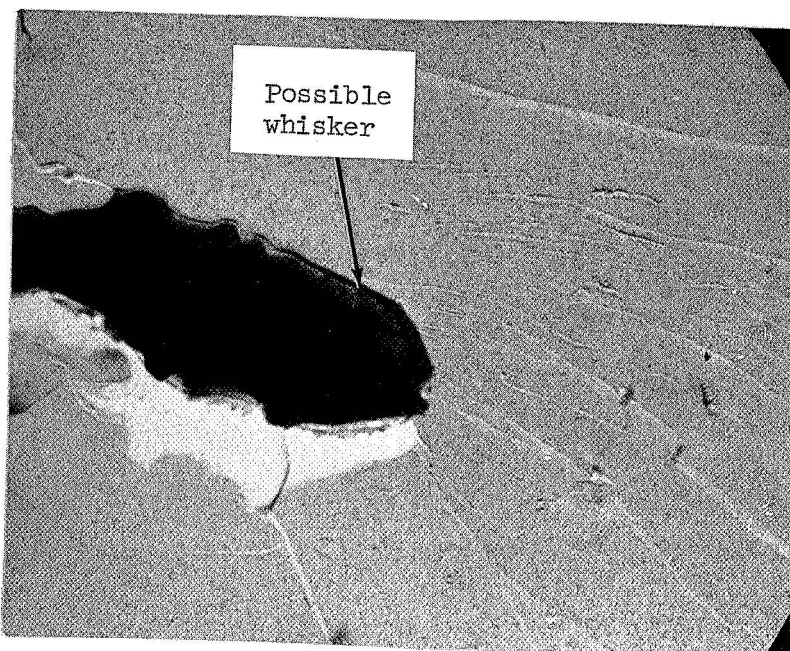
#70375                                       30,000X

Figure 32.   SiC Whisker in Si3N4 Billet 1262 Showing Interference
             in the Propagation of the Crack Front Around it when
             Fractured at Room Temperature.

TABLE 9

IMPACT TEST RESULTS FOR COMPARISON MATERIALS

| Billet | Material | Impact Strength in.-lbs. | | | | | Impact Strength J | | | | |
|---|---|---|---|---|---|---|---|---|---|---|---|
| | | Room Temp. | 2000°F | 2100°F | 2300°F | 2400°F | R.T. | 1366°K | 1422°K | 1533°K | 1589°K |
| Carbitex+ | | 10.35 | 8.25 | - | - | 8.65 | 1.225 | 0.933 | - | - | 0.966 |
| KT SiC+ | | 0.696 | 0.516 | - | - | 1.96 | 0.0786 | 0.0583 | - | - | 0.221 |
| Graphite Cloth in Graphite Matrix | | | | | | | | | | | |
| | Impact ⊥ to cloth | 14.5 (scuffed off) | 0.805 | - | - | 0.696 | 1.64 | 0.091 | - | - | 0.0786 |
| | Impact ∥ to cloth | 9.24 | 0.456 | - | - | 0.576 | 1.041 | 0.0515 | - | - | 0.065 |
| Graphite filaments unidirectional | | 1.09 ∥ | 0.731 ⊥ | - | - | 0.887 ⊥ | 0.123 ∥ | 0.0826 | - | - | 0.100 ⊥ |
| B1900 | | - | 108 | 65.6 | 11.59 | - | - | 12.2 | 7.41 | 1.31 | - |
| X40 - Angle specimen bent to | - | | 134° | 126° | 122° | - | - | 134° | 126° | 122° | - |

∥ parallel with fibers  
⊥ perpendicular to fibers  
+ obtained from Carborundum Corp.

Figure 33. Stress-Strain Curve for 1D Graphite
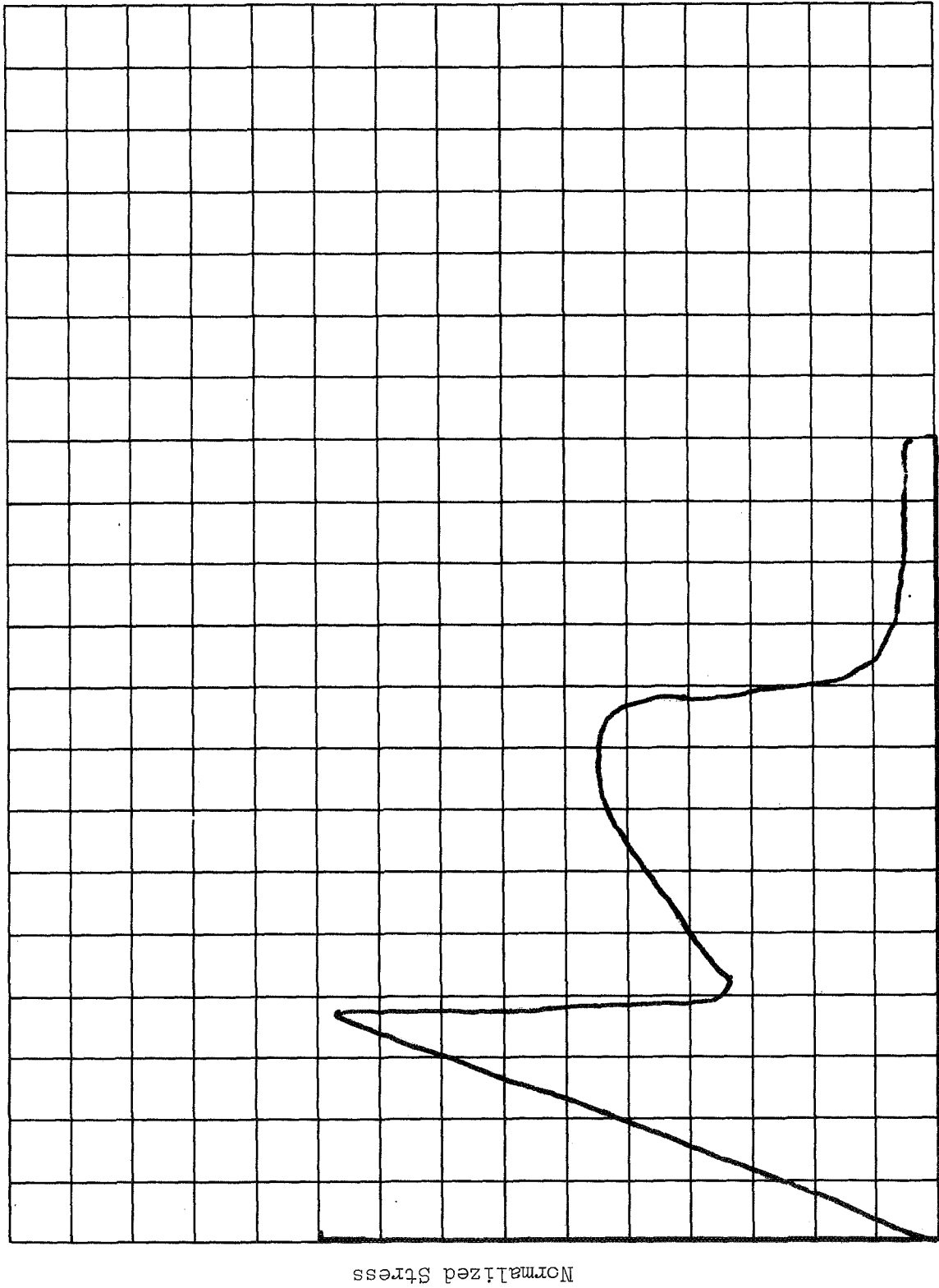
Normalized Strain

Normalized Stress

2000 and 2400°F on the basis of promise shown in the other tests. These were SiC (1233) and Si$_3$N$_4$ (1251) and these two materials with additives of SiC whiskers (1316 and 1262, respectively). Material from two other Si$_3$N$_4$ billets (1401 and 1407) was also used for evaluation of short-time strength from room temperature up to 2400°F (1589°K). Some testing was also done on commercially available SiC and Si$_3$N$_4$ bodies and on two superalloys, B1900 and X-40, for comparative purposes.

All testing was done in four-point flexure; however, there were some differences in the various test units employed which have some influence on the test results. Two stress-rupture stands with resistance furnaces were used; all of the stress-rupture tests were in air. The specimens were 1-3/4 x 0.100 x 0.200 inches and the outer knife edge span was 1.500 inch and the inner knife edge span was 0.500 inch. The predetermined load was applied smoothly in a few seconds with a cam accuator on the load bearing lever arm. Strain was not measured for these tests; a cut-off switch on the lever was utilized to detect and record failure. The 2000°F (1366°K) unit utilized Al$_2$O$_3$ knife edges; platinum foil spacers were used between the knife edge and specimen to reduce the probability of reaction or sticking. Because of the greater oxide formation and reactivity problems, the 2400°F (1589°K) unit had hot pressed SiC knife edges and no foil was used.

Additional short time tests were done in two different tungsten heating element test units requiring argon atmospheres. Where possible, specimens of the same size were tested in a unit built into a Centorr, tungsten element furnace. The load blocks were HfC with a 1.500 inch outer span and a 0.500 inch inner span. This had a constant speed cross-head drive which was set to provide an outer fiber strain rate of about $3 \times 10^{-5}$ sec$^{-1}$.

In some instances material limiations forced the use of smaller specimens which were 7/8 x 0.050 x 0.100 inches. These were tested in an inductively heated unit which employed HfB$_2$ loading rods with an outer span of 0.750 inches and an inner span of 0.250 inches. This provides a constant load rate which was set to provide a nominal strain rate of about $10^{-4}$ sec$^{-1}$ assuming elastic behavior.

All of the results were analyzed using the elastic beam formula of:

$$\sigma = \frac{3 \ Pa}{bh^2} \tag{3}$$

where $\sigma$ = transverse rupture strength in psi
$\quad$ P = load, in pounds required to fracture
$\quad$ b = specimen width in inches
$\quad$ h = specimen thickness in inches

For a dead load test where plastic deformation occurs an indication of the deviation from this formula can be obtained from the approximate equation for the steady-state stress:

$$\sigma = \frac{Pa}{bh^2} \ (2 + m) \tag{4}$$

where m is the strain rate sensitivity exponent. For metals, m is
typically 0.2 to 0.3 so the stress will drop from its initial value to a
value near that given by equation (4). For ceramics, m is typically between
0.5 and 1.0 so that there is often only a small error difference between
the actual steady-state stress and the elastic stress.

### 1. Result for SiC

Stress-rupture tests were run on SiC specimens from billets 1316
and 1233, with and without SiC whisker additions; a few short time tests in
argon were also done to provide base-line data. The results are presented
in Figures 34 and 35 as log-log plots of the stress versus time to rupture;
for the short time tests the total test time was plotted versus the fracture
stress. The emphasis was on the behavior out to 100 hours and tests were
discontinued if fracture had not occurred after this time.

The stress-rupture test data do not extrapolate back through the
short time test data, but rather, to be somewhat lower, especially at $2400^\circ$F
($1589^\circ$K). The limited data preclude a rigorous treatment of this, but is
undoubtedly caused by a difference in testing procedure between the short
time tests in argon and the stress rupture testing in air.

The material made with whiskers had a short time strength about
25% lower than that without whiskers. The stress rupture curves, however,
were found to be flatter especially at the higher temperature when the
curves in Figures 34 and 35 were compared. The microstructural causes for
this cannot be unequivocably established. The microstructures indicated
that the columnar features are coarser for the material with the whiskers
(see Figures 4 and 12). However, fractographs indicated that these large
features are not the basic structural features, but are made up of apparent
grains of about 2 to 3 $\mu$m which are of uncertain character. If the large
columnar features are structurally significant then it seems reasonable
the coarser size may contribute to a lower initial strength for the material
made with whiskers; this, however, cannot be accepted as demonstrated. As a
result of this uncertainty about the grain size influence, it is difficult
to assess the direct affect of the whiskers.

For comparative evaluation some of the high temperature grade of
KT-type SiC was obtained.* The short time strength was found to be about
26 Ksi (1.79 x $10^8$ N/m$^2$). The specimens were found to be more reactive
with Pt so that the test data at $2000^\circ$F ($1366^\circ$K) were felt to be excessively
low and are not reported; the increased activity is attributed to the free
Si in the KT material. At $2400^\circ$F ($1589^\circ$K) the stress rupture strength was
higher than expected and incremental increases in load were required because
of limited specimens; a specimen survived in excess of 100 hours at 20.5 Ksi
(1.41 x $10^8$ N/m$^2$) after considerable exposure at lower stresses. Examination
of the specimen after cooling revealed evidence of more sticking to the
knife edges because of the oxide than was seen with other materials; this
may have the effect of somewhat reducing the moment on the specimen, but a
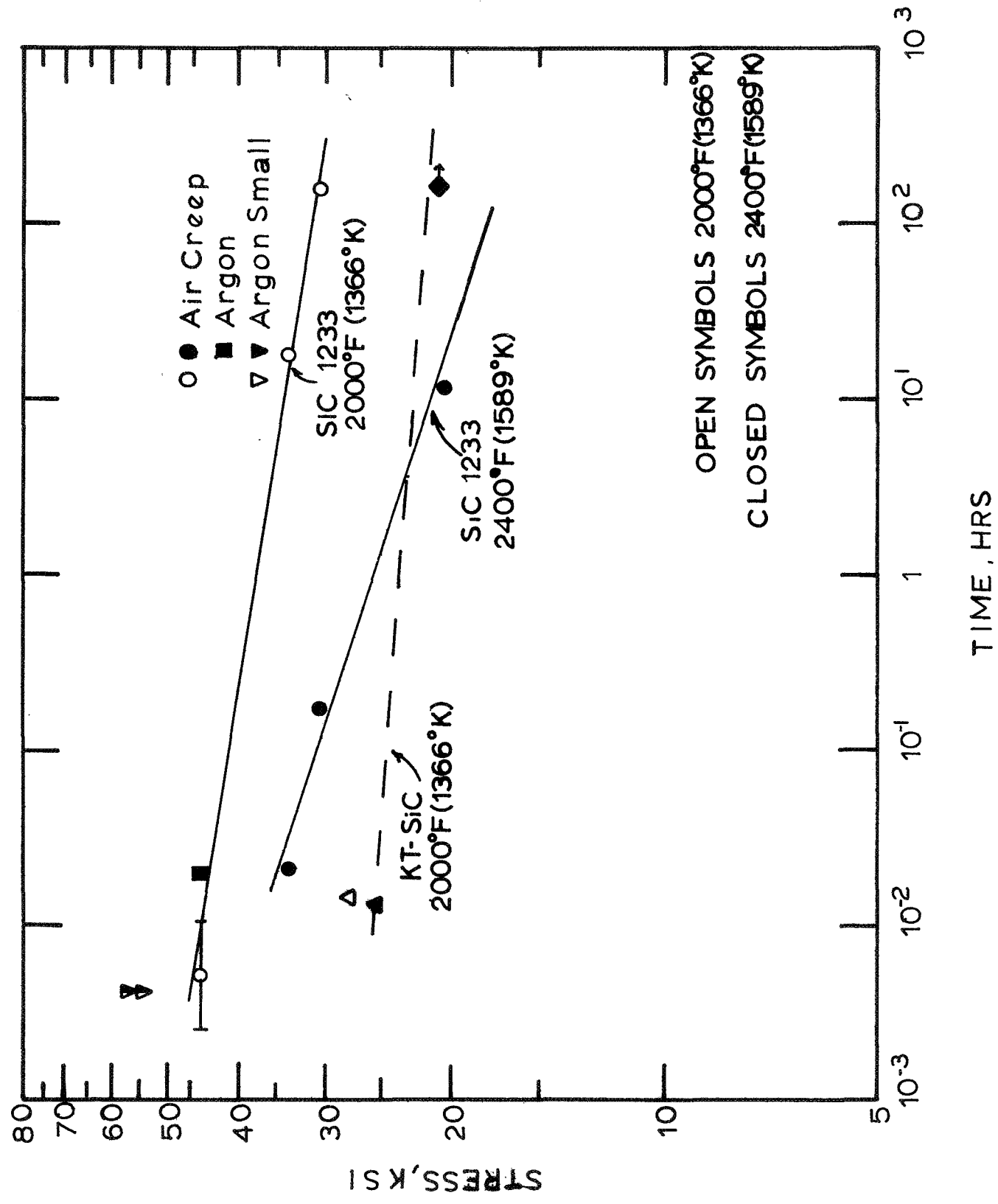
---

* Carborundum Co.

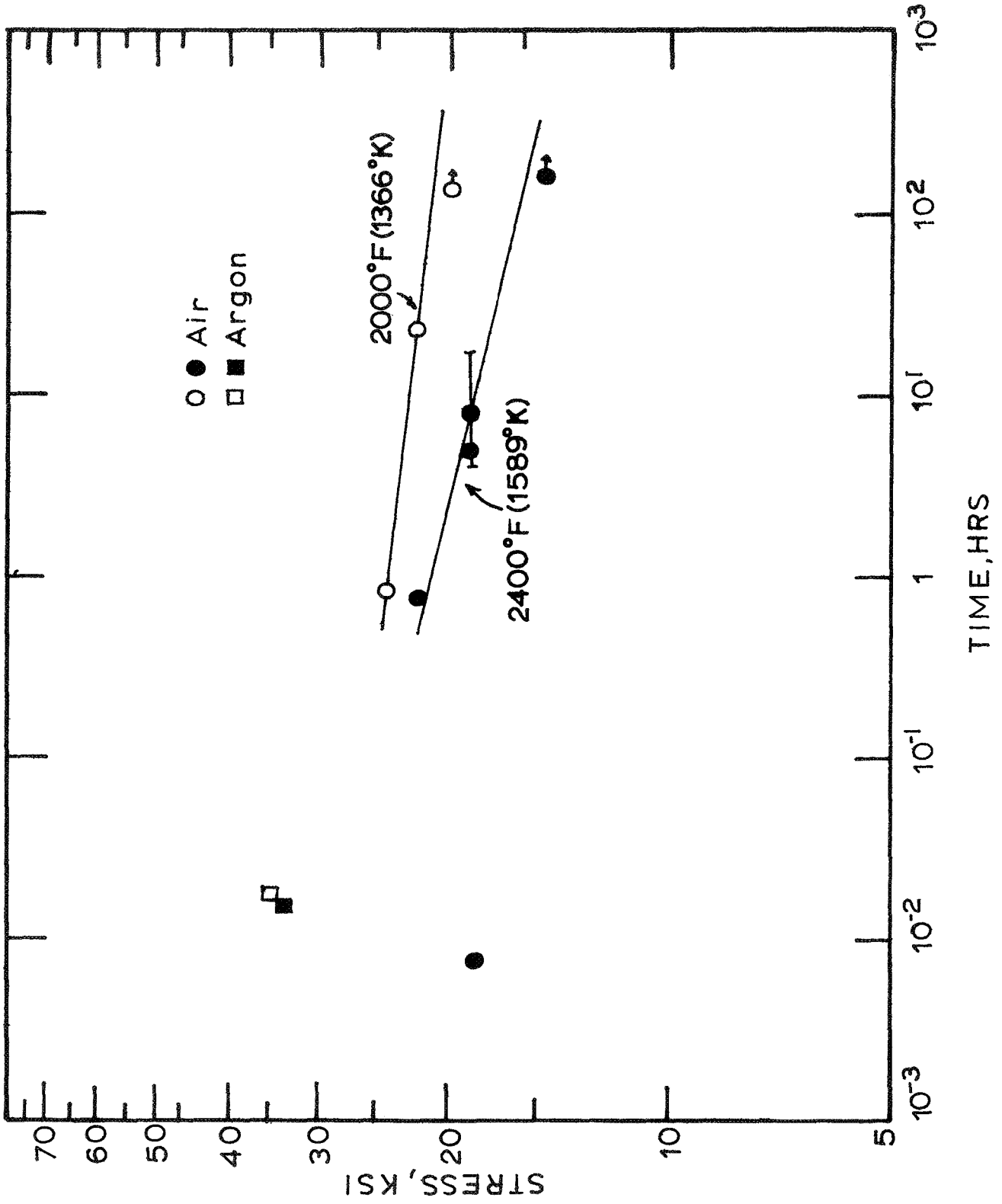Figure 34. Stress-Rupture Results for SiC. (Billet 1233) KT-SiC.

Figure 35. Stress-Rupture Results for SiC + SiC Whiskers (Billet 1316).

large drop in stress cannot be rationalized at this time. This flatter stress-rupture curve at 2400°F (1589°K) in comparison with hot pressed material, may be explained in terms of the coarser grain size of the KT-SiC. It may also be speculated that the hot pressed material has more residual second phase (presumably alumina-rich) at the boundaries which begins to soften at these temperatures and causes lower rupture strength; no other evidence for this has been seen or reported, however.

No strain measurements were made during the tests. After removal the curavture of the specimens was estimated and converted into outer fiber strains for the various specimens. The hot pressed materials exhibited virtually no deformation at 2000°F (1366°K) and a barely detectable curvature $\sim$ 0.01% after testing at 2400°F (1589°K). The KT specimen had a slight curvature ( $\epsilon \approx 0.1\%$) after testing at 2400°F (1589°K).

## 2. Results for $Si_3N_4$

Specimens of $Si_3N_4$ (1251) and $Si_3N_4$ with SiC whiskers (1262) were tested in a similar fashion to the SiC materials. The results are plotted in Figures 36 and 37. It can be seen that the base material had a much flatter stress-rupture curve than anticipated at 2000°F (1366°K); incremental loading of a specimen was necessary to obtain fracture in the available times. Examination of this material afterwards indicated no degradation from reaction with the Pt. The specimen did have a rather heavy oxide layer on it. Only a slight amount of curvature was evident at 2000°F (1366°K) ($\epsilon < 0.1\%$). The very short time stress rupture failure is suspect as a result of uncertainty about impact or other problems during loading. At 2400°F (1589°K) the stress rupture strength was much reduced, having fallen below that of the SiC materials. Appreciable bending could be detected in the specimens ($\epsilon \sim 0.2\%$) after testing at 2400°F (1589°K). The 2400°F (1589°K) specimens had a heavy glassy oxide layer on them, but reaction with the SiC knife edge was not a problem.

The addition of the SiC whiskers (billet 1262) resulted in a slight reduction in short time strength at 2000°F (1366°K), but caused a considerable reduction in strength at 2400°F (1589°K) and much reduced stress-rupture resistance at both temperatures. This exhibited slightly more strain at 2000°F (1366°K) and exhibited about 1.0% strain at 2400°F (1589°K). The material with whiskers had a finer grain size ( 1 μm compared to 2.5 μm); this suggests that the lower stress rupture strength may be the result of an increased effect of grain boundary weakening and sliding. It was noted that the SiC addition substantially eliminated the heavy oxide layer at 2000°F (1366°K) and reduced the thickness at 2400°F (1589°K).

A series of short time tests from room temperature to 2400°F (1589°K) were done for two additional hot pressed material (1401 pressed from $\alpha$ -$Si_3N_4$ powder, and 1407 with an $MgAl_2O_4$ additive); both had sub-micron grain sizes. A similar series was also run on some material which was obtained from Joseph Lucas Ltd. at the end of the program; only a small amount of this was available so small specimens were used.

The results are plotted in Figure 38. It can be seen that a marked drop in strength occurs at about 1800-2000°F (1255-1366°K); this is known to
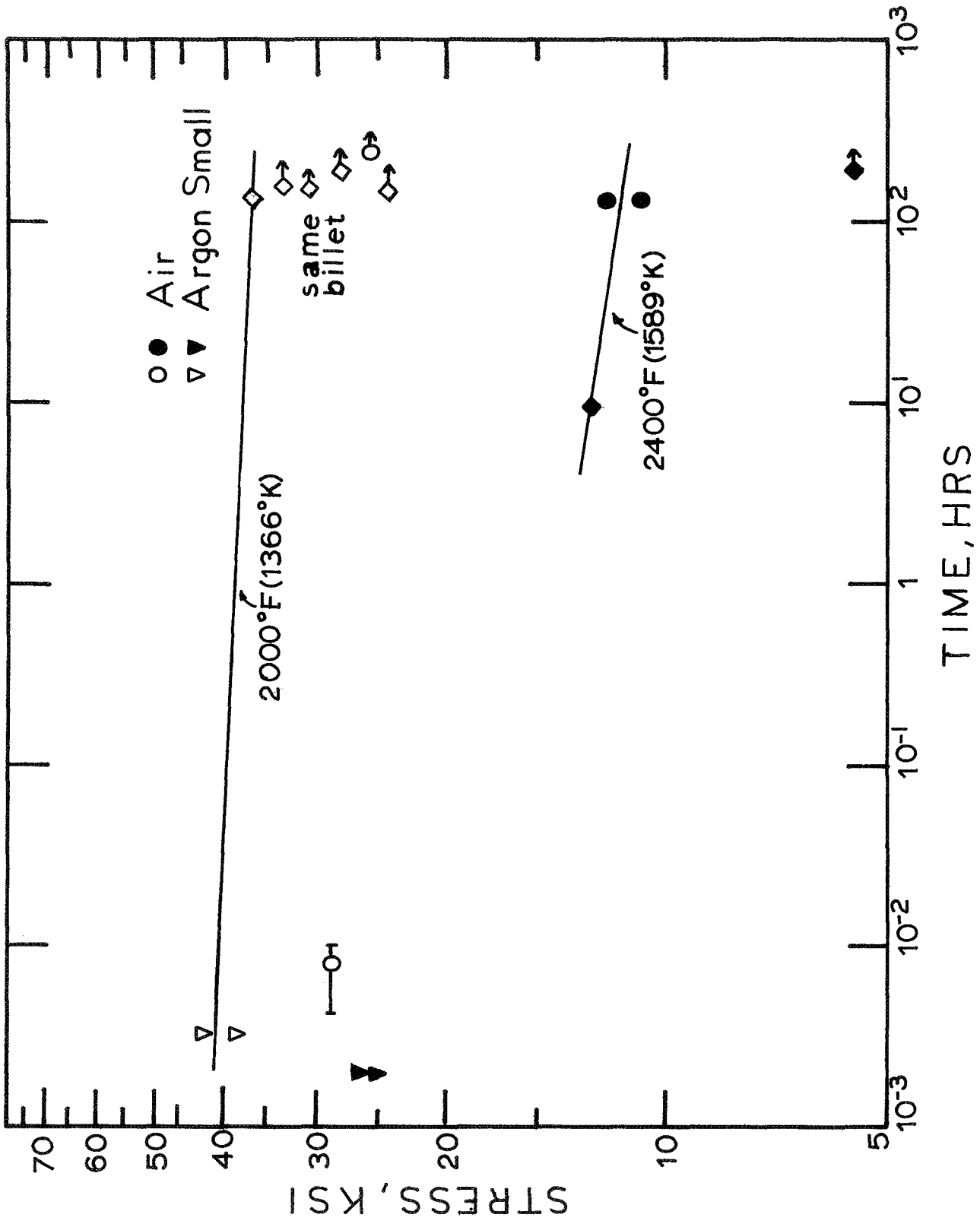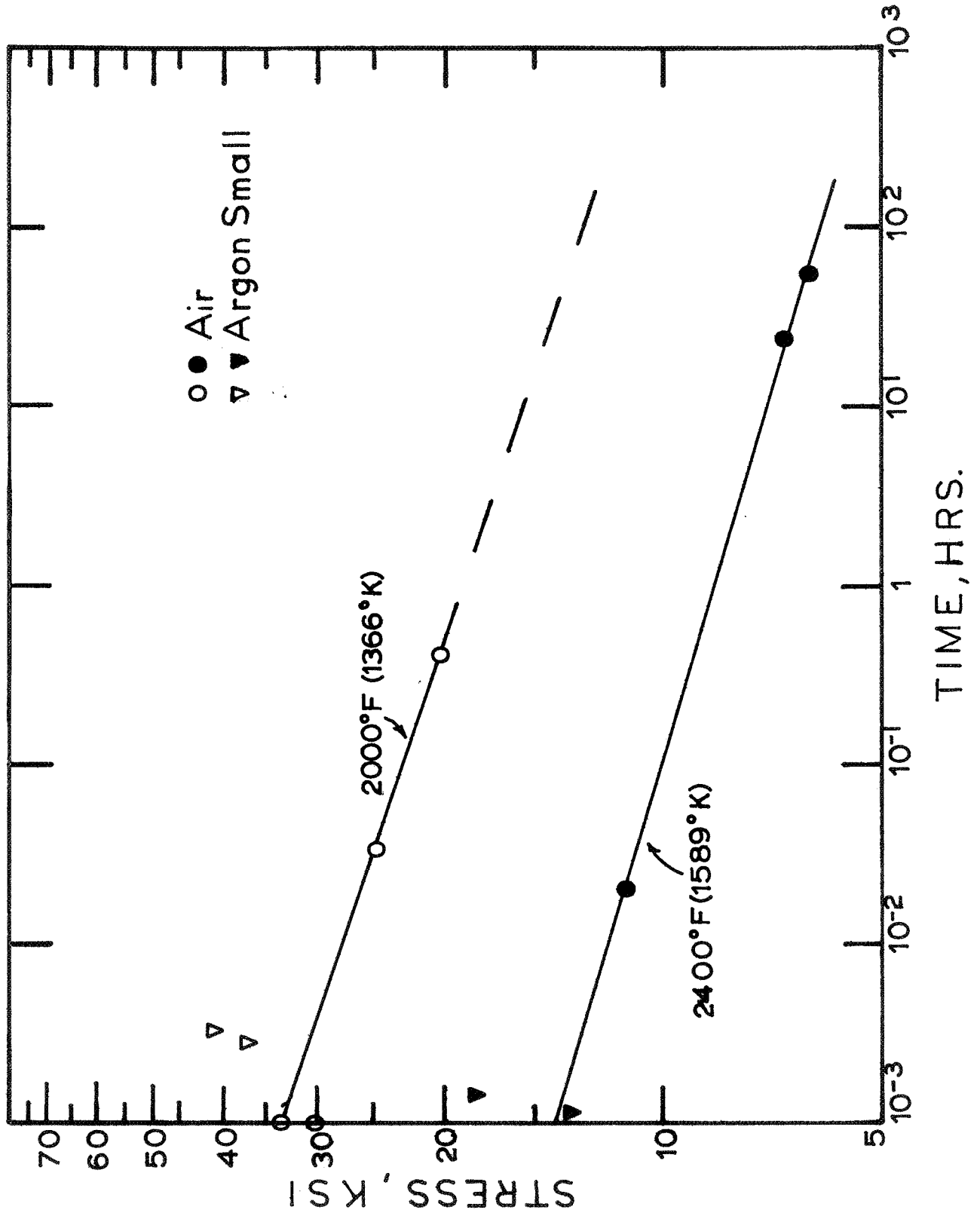
Figure 36. Stress-Rupture Results for Si3N4 (Billet 1251).

Figure 37.  Stress Rupture Results for $Si_3N_4$ + SiC Whisker (Billet 1262).

be strongly influenced by the additives used which are presumed to remain
as residual grain boundary phases or impurities; the more rapid drop of
the spinel bearing material is in keeping with this. It should be noted
that the rate of decrease was less for the small specimens tested at a
higher constant load rate. The shape of the curve of the Lucas material
between 800°F (699°K) and 1600°F (1144°K) was chosen in part on the basis
of information from the supplier.

Examination of the fractured specimens indicated a difference in
behavior at 2400°F (1589°K) for the slower rate tests. The gage length had
additional cracks in it and the fracture surface gave evidence of considerable
controlled growth of the crack before the catastrophic brittle fracture
initiated. This effect was much less evident in the faster tests. Oxidation
obscured any such evidence in the stress-rupture tests. This type of behavior
is consistent with an impurity induced boundary weakening and sliding leading
to intergranular separation and failure. Further support for this argument
is obtained by the behavior of reaction sintered material which does not
have the additives used in hot pressing. Data from the literature[15] for
material of 2.5 g/cc density is included in Figure 38. It can be seen that
the strength is held to much higher temperatures without a large drop.

## 3. Comparison of Data with Current Metal Alloy Systems

For comparative purposes the 100-hour rupture stress was taken
for all of the materials tested and plotted in Figure 39. Also included
for comparison are literature data for three superalloys of different types,
B-1900, X-40 and TD-Ni. Estimated values of the curves for the ceramics at
lower temperatures are shown for further comparison; these were estimated by
extrapolating back from the data using various low temperature strength data
and assumptions about behavior at the lower temperatures. These should be
used only for general comparative purposes.

In order to establish confidence in comparisons of these flexural
measurements and the tensile measurements commonly used for metals a few
four-point bend tests on B-1900 and X-40 material were planned. Individual
tests were done at 2000°F (1366°K) on B-1900 and X-40; in both cases the
specimens bottomed out at approximately 3% outer fiber strain before failure
occurred. As a result, further testing was not done. Testing was not
attempted at 2400°F (1589°K) because this is at or above the solidus for these
alloys. The test conditions for the above two materials at 2000°F (1366°K)
were 13.5 Ksi (9.28 x 10$^7$ N/m$^2$) for 110 hours for B-1900 and 9.8 Ksi (6.74 x
10$^7$ N/m$^2$) for 13 hours for X-40. Comparison with Figure 39 shows these numbers
to be somewhat in excess of the curves given. Referring back to equations (3)
and (4) the effect of the plastic deformation on the actual outer fiber stress
can be seen; by estimating 'm' at about 0.25 (typical for this class of
material) the actual stress would only be about 75% of that calculated. This
correction brings the numbers into fair agreement with those plotted in
Figure 39. These problems are not so significant for the ceramics since
'm' values are usually near unity; as a result, the effect of plastic de-
formation on the calculated stress is not so great.

At 2000°F (1366°K) the $Si_3N_4$ had the highest rupture strength of
all the materials tested. At 2400°F (1589°K) the SiC based materials were
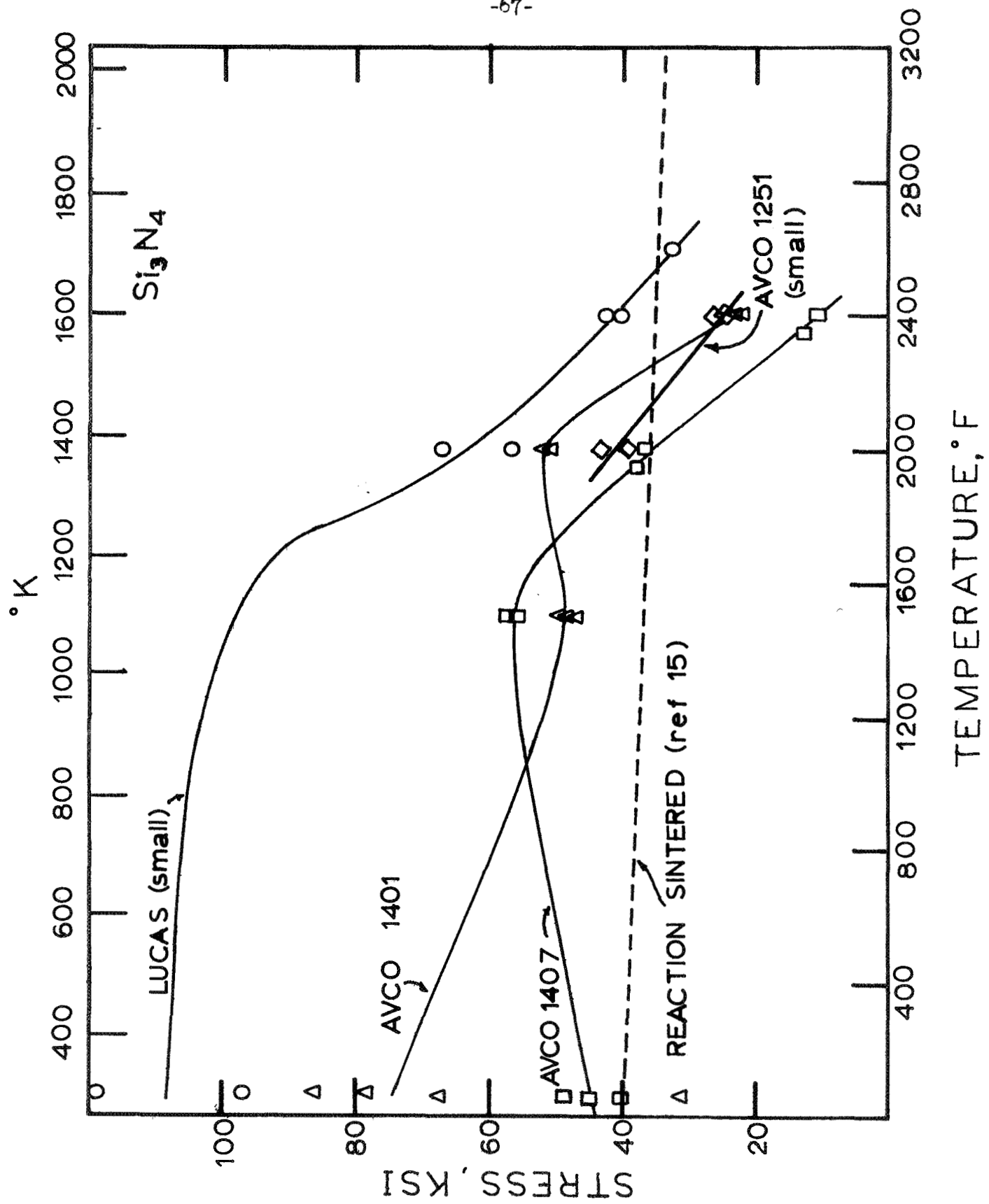superior. Indications are that reducing the residual grain boundary

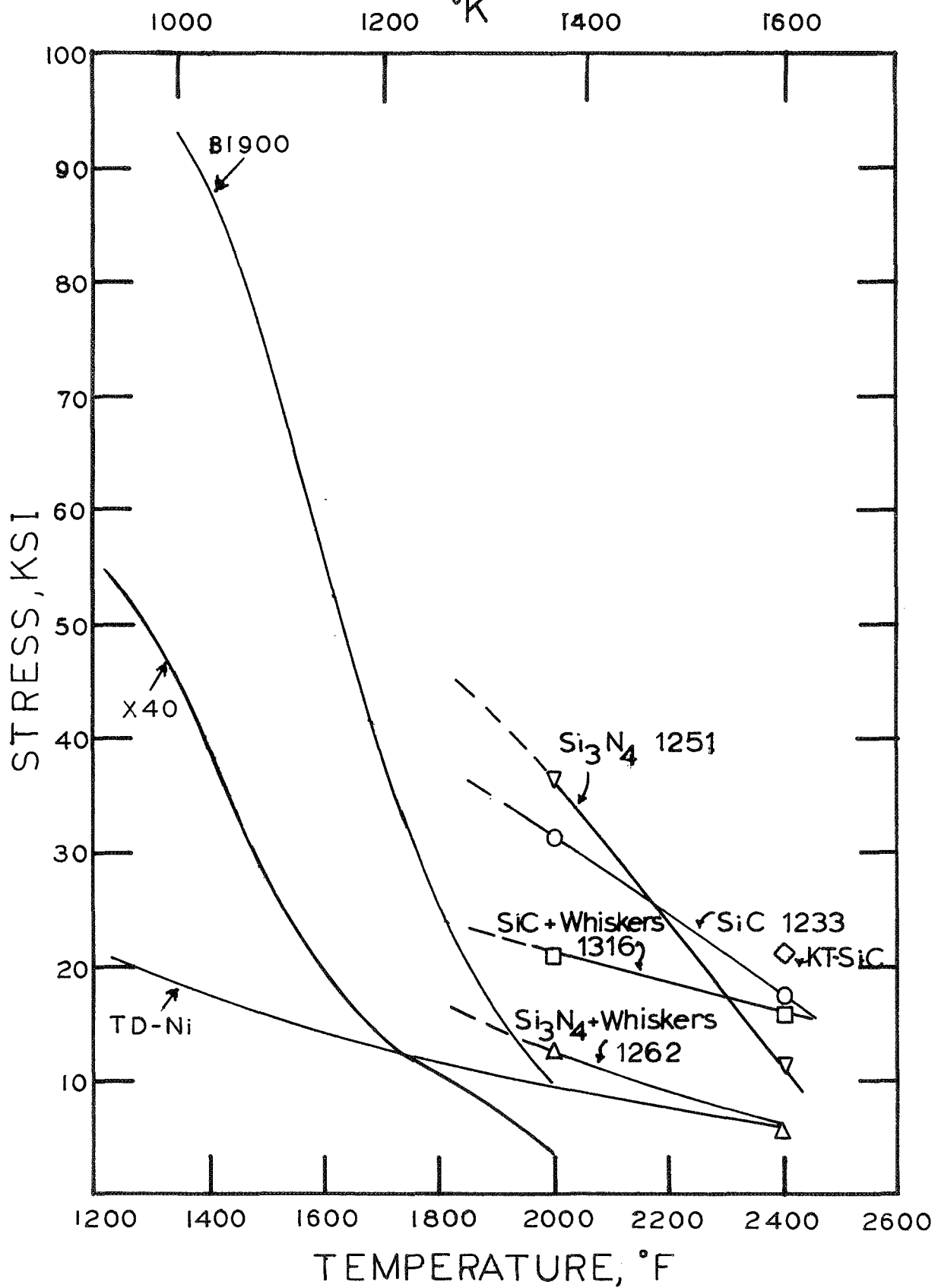Figure 38. Short-Term Fracture Stress versus Temperature for Some Materials.

Figure 39. 100 Hour Rupture Stress versus Temperature for a
Number of Ceramic and Metal Alloy Systems.

impurities would extend the temperature capability of $Si_3N_4$; this would be expected to result in substantial improvements in the 2400°F (1589°K) stress rupture strength. The higher rupture strength of the KT grade at 2400°F (1589°K) suggests that a similar grain boundary impurity problem may exist for the SiC; this is a more tentative position for this material.

For both the SiC and $Si_3N_4$ it is difficult to assess the direct affect of the whiskers because of differences in final grain size, density and the possibility of subtle differences in grain boundary constituents. For both base materials the strengths were reduced by the whisker additions; this may, however, have resulted from indirect effects.

The work reported indicated that in terms of most of the critical requirements, ceramic composites based on SiC or $Si_3N_4$ show promise for use in low stress areas of gas turbines at least up to 2400°F (1589°K). Despite being inherently brittle materials, their fracture toughness has been improved by additions of SiC whiskers. When these additions can be optimized, it is anticipated that the composites can compete successfully with metals for stator vanes in advanced gas turbines.

## V. CONCLUSIONS

SiC and $Si_3N_4$ made by hot pressing and having certain sintering aid additions are capable of successfully surviving at least 100 cycles in a simulated gas turbine stator vane environment at 2400°F (1589°K). Additions of SiC whiskers do not have a marked effect on the thermal stability/shock resistance of either SiC or $Si_3N_4$. In terms of impact strength there is a marked increase when SiC whiskers are added to either ceramic to form a composite. In the case of SiC an increase from 0.55 in lbs. (0.062J) to 1.6 in lbs. (0.18J) at room temperature and from 0.64 in lbs. (0.07J) to 1.35 in lbs. (0.153J) at 2400°F (1589°K). For $Si_3N_4$ the increase was from 1.05 in lbs. (0.119J) to 1.33 in lbs. (0.15J) at room temperature and from 1.31 in lbs. (0.15J) to 1.68 in lbs. (0.19J) at 2400°F (1589°K).

Thus, the impact strength of SiC does not change much at high temperature compared with the room temperature values. Silicon nitride has a higher impact strength than SiC. The strength of $Si_3N_4$ also increased when heated to 2000°F (1366°K) and 2400°F (1589°K).

If such a whisker composite based on either SiC or $Si_3N_4$ can be optimized in terms of whisker size and aspect ratio, the optimum percentage additive, and also the alignment of the whiskers in the appropriate direction with respect to the applied stress, increases are anticipated in impact strength in excess of the 300% already obtained.

# VI. REFERENCES

1.  R.S. Truesdale, J.J. Swica and J.R. Tinklepaugh, "Metal Fiber Reinforced Ceramics," WADC TR-58-452 (December 1958).

2.  J.J. Swica, W.R. Hoskgus, B.R. Goss, J.H. Connor and J.R. Tinklepaugh, "Metal Fiber Reinforced Ceramics," WADC TR-58-452, Part II, (January 1960).

3.  J.R. Tinklepaugh, B.R. Goss, W.R. Hoskgus, J.H. Connor and D.D. Button, "Metal Fiber Reinforced Ceramics," WADC TR-58-452, Part III, (November 1960).

4.  D.H. Bowen, "Fiber Reinforced Ceramics," Fibre Science and Technology, 1, No. 2, 85 (1968).

5.  J.W. Orner, "The Quantitative Significance of Non-destructive Evaluation of Graphite and Ceramic Materials," Technical Report AFML-TR-70-205, August 1970.

6.  R.A. Alliegro, L.B. Coffin and J.R. Tinklepaugh, J. Am. Ceram. Soc., 39, 386 (1956).

7.  G.G. Deeley, J.M. Herbert and N.M. Moore, Powder Met., No. 8, 145 (1961).

8.  P.L. Pratt, "Mechanical Properties of Engineering Ceramics," ed. Kriegal and Palmout, Interscience (1961).

9.  C.E. Wicks and F.E. Block, "Thermodynamic Properties of 65 Elements -- Their Oxides, Halides, Carbides and Nitrides," Bureau of Mines, Bulletin 605 (1963).

10. H.L. Schick, "Thermodynamics of Certain Refractory Compounds," Vol. II, p. 191, publ. American Press, New York (1966).

11. E.K. Storms, "A Critical Review of Refractories, Pt. II, Selected Properties of Group -4a, -5a, -6a Nitrides," LAMS-2674, (Pt. II), (1962).

12. M. Hansen, "Constitution of Binary Alloys," publ. McGraw-Hill Book Co., New York (1958).

13. R.J. Lumby and R.F. Coe, "The Influence of Some Process Variables on the Mechanical Properties of Hot Pressed Silicon Nitride," presented at the British Ceramic Society Meeting, London, (December 18-19, 1968).

14. P. Grieveson, K.H. Jack and S. Wild, "The Crystal Chemistry of Ceramic Phases in the Silicon-Nitrogen-Oxygen and Related Systems," Progress Report No. 5, Ministry of Defense Contract N/CP.61/9411/67/4B/MP.387 (June 1970).

## VI. REFERENCES (Concl'd)

15. A.G. Evans and R.W. Davidge, J. Mat'l. Science, 5, 314 (1970).

16. E.V. Clougherty and E.T. Peters, "Research and Development of Refractory Oxidation Resistant Diborides," Part II, Vol. III, Technical Report AFML-TR-68-190, Part II, Vol. II (January 1970).

17. T.J. Rockett and W.R. Foster, J. Am. Ceram. Soc., 48, 78 (1965).

APPENDIX A

CALIBRATION OF HOT PRESSING SET-UP


A calibration was conducted in the 75 ton (6800 Kg) Dake press using a $6\frac{1}{2}$-inch (16.5 x $10^{-2}$m) O.D., 2-inch (5.08 x $10^{-2}$m) I.D., $7\frac{1}{2}$-inch (19 x $10^{-2}$m) long ATJ die with a 3/4-inch (1.9 x $10^{-2}$m) high Norblack powder charge and a $1\frac{1}{2}$-inch (3.81 x $10^{-2}$m) deep hole in the die wall for the sight tube. Two pyrometers were used to sight simultaneously through a hole in the piston train to the powder and through the normal sight tube into the die wall hole. Care was taken to check for differences between the pyrometers, mirror corrections, window corrections and to ensure argon gas flow to keep the sight holes clear. The calibration was performed over the range of 3317°F (2098°K) to 4136°F (2653°K) and the results are shown in Table Al.

The results indicated that after making the appropriate corrections to the indicated temperatures, the difference between the temperature of the Norblack charge and the sight tube varied between -12.5°F to 41.5°F (-7 to +23°K).

The -48.5°F (-27°K) value at 4136°F (2653°K) was a transient value due to the rapid rate of heating at this point in the experiment.

## TABLE A-1

TEMPERATURE CALIBRATION OF 2-INCH ($5.08 \times 10^{-2}$m) DIAMETER HOT PRESSING DIE

(All corrections made except for sight window)

| Pyro #2, Sight Tube $T_s$ °K | Pyro #1, Cavity $T_c$ °K | $(T_c - T_s)$ $\Delta$ °K | Remarks |
|---|---|---|---|
| 2098 | 2111 | 13 | Med. scale, temp. partially stab. #1 pyro. |
| 2123 | 2173-12 = 2161 | 38 | High scale, temp. partially stab. |
| 2308 | 2353-12 = 2341 | 33 | High scale, temp. partially stab. |
| 2553 | 2573-12 = 2561 | 8 | High scale, temp. partially stab. |
| 2653 | 2653-12 = 2641 | -12 | High scale while heating |

(All corrections made including sight window)

| | | | |
|---|---|---|---|
| 2098 + 15 = 2013 | 211 | -2 | |
| 2123 + 15 = 2138 | 2173-12 = 2161 | 23 | |
| 2308 + 15 = 2323 | 2353-12 = 2341 | 18 | |
| 2553 + 15 = 2568 | 2573-12 = 2561 | -7 | |
| 2653 + 15 = 2668 | 2653-12 = 2641 | -27 | |

(Corrections)

1. Pyro #2 - 12°K higher than pyrometer #1.
2. Sight window 15°K absorption.

## APPENDIX B

### CALIBRATION OF THERMAL SHOCK/THERMAL STABILITY RIG

The thermal stability/thermal shock rig described in Section IV.C · was calibrated in terms of the heating and cooling rates. Figure B-1 shows the cooling rate and heating rate of a typical cycle. The specimens were cooled from $2400^\circ F$ ($1589^\circ K$) to $250^\circ F$ ($394^\circ K$) in $2\frac{1}{2}$ minutes. The heating rate can be summarized thus:

to within $30^\circ F$ ($16.6^\circ K$) of original temperature - $6\frac{1}{2}$ minutes

to within $30^\circ F$ ($11.1^\circ K$) of original temperature - 8 minutes

to within $10^\circ F$ ($5.55^\circ K$) of original temperature - $13\frac{1}{2}$ minutes

to within $0^\circ F$ ($0^\circ K$) of original temperature -     15 minutes

The flame remains remarkably constant for many hours and the specimen temperature was shown to vary $\pm 6^\circ F$ ($3.33^\circ K$) only for tens of hours. The specimens ran at a temperature characteristic of their position in the holder. Typical temperatures as determined optically are:

| Position | Temperature, $^\circ F$ | Temperature, $^\circ K$ |
|----------|------------------------|-------------------------|
| 1 | 2392 | 1585 |
| 2 | 2408 | 1593 |
| 3 | 2421 | 1601 |
| 4 | 2401 | 1589 |
| 5 | 2376 | 1575 |

These temperatures are of the trailing (wide) edge of the specimen, and it is found that the leading (narrow) edge of the specimen is hotter than the former by approximately $20^\circ F$ ($11.1^\circ K$).

Figure B-1. Thermal Stability Calibration
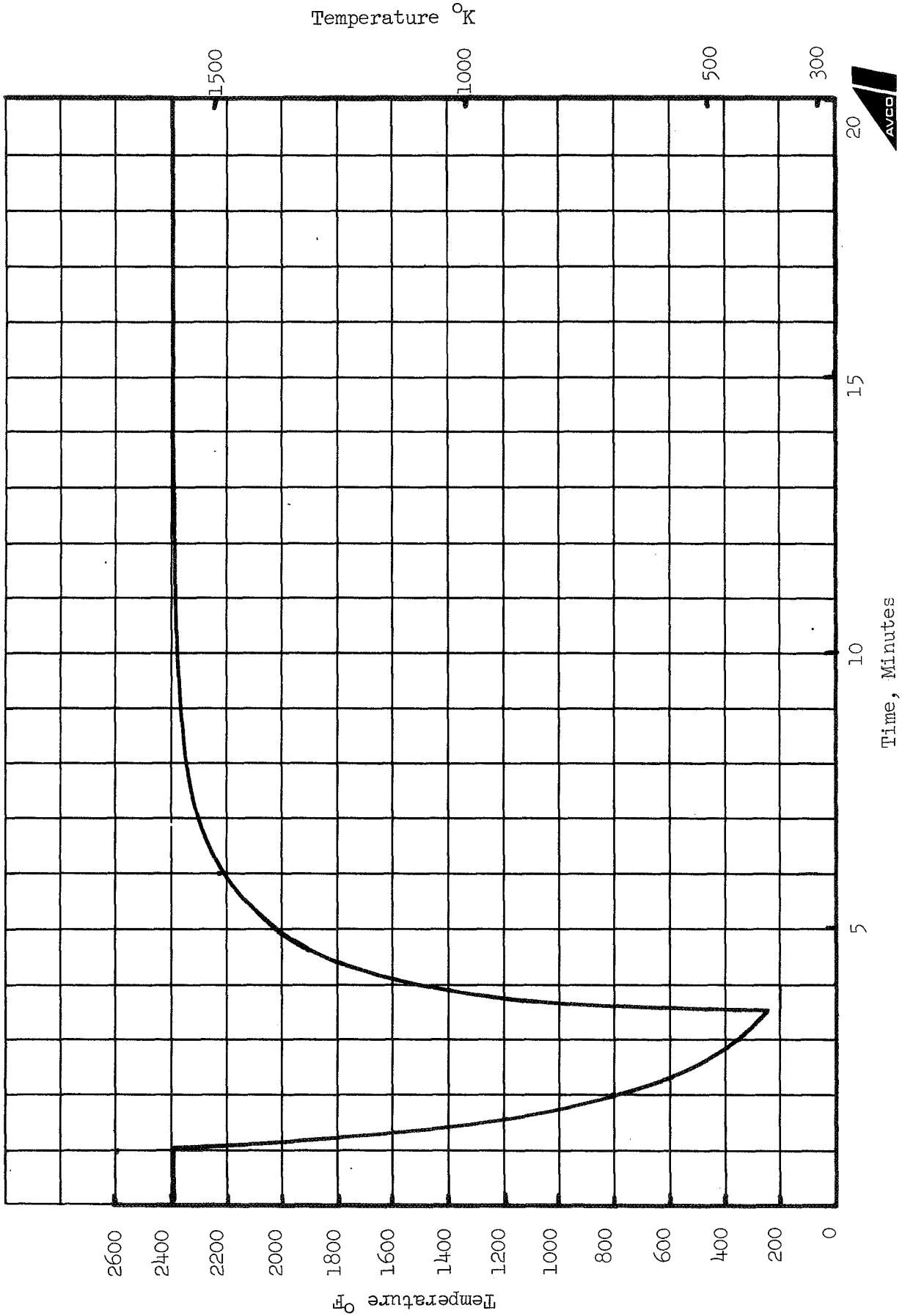
| Addressee | No. Copies |
|---|---|
| NASA Headquarters | |
| 600 Independence Avenue, S.W. | |
| Washington, D.C. 20546 | |
| Attention: N.F. Rekos (RAP) | 1 |
| G.C. Duetsch (RR-1) | 1 |
| | |
| FAA Headquarters | |
| 800 Independence Avenue, S.W. | |
| Washington, D.C. 20553 | |
| Attention: General J.C. Maxwell | 1 |
| | |
| NASA Scientific & Technical Information Fac. | |
| Post Office Box 33 | |
| College Park, Maryland 20760 | 6 |
| | |
| NAS Lewis Research Center | |
| 21000 Brookpark Road | |
| Cleveland, Ohio 44135 | |
| Attention: | |

| | | |
|---|---|---|
| 1. | Aeronautics Procurement Section, M.S. 77-3 | 1 |
| 2. | Technology Utilization Office, M.S. 3-19 | 1 |
| 3. | Library, M.S. 60-3 | 3 |
| 4. | Report Control Office, M.S. 5-5 | 1 |
| 5. | G.M. Ault, M.S. 3-13 | 1 |
| 6. | J. Merutka, M.S. 49-1 | 1 |
| 7. | R. Hall, M.S. 105-1 | 1 |
| 8. | J. Weeton, M.S. 49-1 | 1 |
| 9. | N. Saunders, M.S. 105-1 | 1 |
| 10. | J. Freche, M.S. 49-1 | 1 |
| 11. | R. Kemp, M.S. 49-1 | 1 |
| 12. | R. Signorelli, M.S. 106-1 | 1 |
| 13. | W. Sanders, M.S. 49-1 | Balance |

Dr. Earl R. Thompson
Chief, Advanced Metallurgy
United Aircraft Research Labs.
E. Hartford, Conn.   06108

General Electric Co.
Research & Development Center
P.O. Box 8
Schenectady, New York   12301
Attn:  Dr. D. Wood

United Aircraft Corp.
Pratt & Whitney Aircraft Div.
Florida Research & Develop. Center
West Palm Beach, Florida
Attn:  R.P. Huggins, Head Librarian

Dr. A.R. Stetson
Solar Division
International Harvester Co.
2200 Pacific Highway
San Diego, Calif.   92112

General Electric Co.
AEG Technical Information Center
N-32, Bldg. 700
Cincinnati, Ohio   45215

Mr. Richard Alliegro
Asst. Director of Research &
Development
Refractories Division
Norton Co.
Worcester, Mass.   01606

Dr. E.V. Clougherty
ManLabs, Inc.
21 Erie Street
Cambridge, Mass.   02139

Mr. John Fenter
MAMC
Metals & Ceramics Div.
Wright-Patterson AFB
Dayton, Ohio

Airesearch Manufacturing Co.
Phoenix Arizona 85034
Attn:  Supervisor, Materials Eng. Dept.

Mr. R.B. Simonson, Mgr.
Applied Materials Dept.
TRW, Inc.
1 Space Park
Redondo Beach, Calif.   90278

Mr. W.M. Powers, Vice President
Marketing
General Technologies Corp.
1821 Michael Faraday Drive
Reston, Virginia   22070

Dr. Peter L. Fleischner, Head
Research and Development
National Beryllia Corp.
Greenwood Avenue
Haskell, New Jersey   07420

Defense Ceramic Information Center
Battelle Memorial Institute
Columbus Laboratories
505 King Avenue
Columbus, Ohio   43201

Dr. F.F. Lange
Westinghouse Electric Corp.
Research and Development Center
Beulah Road Churchill Borough
Pittsburgh, Pennsylvania   15235

Dr. D.E. Harrison
Westinghouse Electric Corp.
Research and Development Center
Beulah Road Churchill Borough
Pittsburgh, Pennsylvania   15235

Dow Chemical Co.
Bldg. 566, Contract Research and
Development
Midland, Michigan   48640
Attn:  Mr. R.F. Helmreich

Consolidated Controls Corp.
Advanced Research and Development
75 Dumont Avenue
Bethel, Conn.   06801
Attn:  Mr. R.E. Engdahl

Systems Research Labs.
7001 Indian Ripple Road
Dayton, Ohio 45440
Attn:  Mr. W. Zulp

Hough Laboratories
708 Rice Street
Springfield, Ohio   45505
Attn:  Mr. R.C. Hough

Garrett Corporation
333 West First Street
Dayton, Ohio   45402

Atlantic Research Corp.
Shirley Highway
Edsall Road
Alexandria, Virginia  22314
Attn:  Mr. H.W. Norton

Aerojet General Corp.
20545 Center Ridge Road
Cleveland, Ohio  44116
Attn:  Mr. W.L. Snapp

Philco Ford Corp.
Aeroneutronic Div.
Ford Road
Newport Beach, Calif.  92663
Attn:  Dr. Martin Fassell

ManLabs, Inc.
21 Erie Street
Cambridge, Mass.  02139
Attn:  Dr. L. Kaufman

Battelle Memorial Institute
505 King Avenue
Columbus, Ohio  43201
Attn:  Dr. Robert Jaffe

Battelle Northwest
Richland, Washington
Attn:  Mr. J.V. McMaster

TRW, Inc.
23555 Euclid Avenue
Cleveland, Ohio  44117
Attn:  Dr. Edward Steigerwald

Midwest Research Institute
425 Volker Blvd.
Kansas City, Missouri  64110
Attn:  Mr. Perry L. Bidstrup

Arthur D. Little, Inc.
15 Acorn Park
Cambridge, Mass.  02140
Attn:  Mr. M.W. Silber

IIT Research Institute
10 West 35 Street
Chicago, Illinois  60616
Attn:  Dr. S. Bortz

Kawecki Berylco Industries, Inc.
P.O. Box 1462
Reading, Pennsylvania  19603
Attn:  Mr. Norman P. Pinto

Admiralty Materials Laboratory
Holton Heath, Poole, Dorset BH16 6JU
England
Attn:  Dr. D.G. Godfrey

Doulton Ind. Products, Ltd.
Technical Ceramics Division
Filleybrooks, Stone, Staffs
England
Attn:  Mr. D.J. Flye

Professor K.H. Jack
Metallurgy Dept.
The University of Newcastle upon Tyne
England

Philco-Ford Corp.
Aeronutronic Division
Ford Road
Newport Beach, Calif.  92663
Attn:  Mr. Tom Place

Materials Research Corp.
Orangeburg, New York  10962

Carborundum Corp.
Research & Developm. Div.
Niagara Falls, New York

Atomic Energy Research Estab.
Materials Develop. Div.
Harwell, Didcot, Berks.
England
Dr. R.W. Davidge

United Kingdom Atomic Energy
Authority,
The Reactor Group
Reactor Fuel Element Labs.
Springfields, England
Attn:  Dr. C.W. Forrest

Dr. J.T. Barnby
Dept. of Metallurgy
The University of Aston in Birmingham
Gosta Green, Birmingham 4
England

Dr. M.J. Sinnott
ARPA Materials Science
1400 Wilson Blvd.
Architects Bldg.
Arlington, Va.  22209